Neurobiology of Disease

# Fragile X Mental Retardation Protein Bidirectionally Controls Dendritic $I_h$ in a Cell Type-Specific Manner between Mouse Hippocampus and Prefrontal Cortex

**Federico Brandalise,[1,2*] Brian E. Kalmbach,[1,2*] Preeti Mehta,[1,2] Olivia Thornton,[1,2] Daniel Johnston,[1,2] Boris V. Zemelman,[1,2] and Darrin H. Brager[1,2]**

[1]Center for Learning and Memory, University of Texas at Austin, Austin, Texas 78712, and [2]Department of Neuroscience, University of Texas at Austin, Austin, Texas 78712

**Channelopathies are implicated in Fragile X syndrome (FXS), yet the dysfunction of a particular ion channel varies with cell type. We previously showed that HCN channel function is elevated in CA1 dendrites of the *fmr1*$^{-/y}$ mouse model of FXS, but reduced in L5 PFC dendrites. Using male mice, we tested whether Fragile X Mental Retardation Protein (FMRPO), the protein whose absence causes FXS, differentially modulates HCN channels in CA1 versus L5 PFC dendrites. Using a combination of viral tools, intracellular peptide, and dendritic electrophysiology, we found that FMRP regulates HCN channels via a cell-autonomous protein–protein interaction. Virally expressed FMRP restored WT HCN channel-related dendritic properties in both CA1 and L5 neurons. Rapid intracellular perfusion of the non-mRNA binding N-terminal fragment, $FMRP_{1\text{-}298}$, similarly restored dendritic function. In support of a protein–protein interaction, we found that FMRP associated with HCN-TRIP8b complexes in both hippocampus and PFC. Finally, voltage-clamp recordings showed that FMRP modulated $I_h$ by regulating the number of functional dendritic HCN channels rather than individual channel properties. Together, these represent three novel findings as to the nature of the changes in dendritic function in CA1 and PFC neurons based on the presence or absence of FMRP. Moreover, our findings provide evidence that FMRP can regulate its targets in opposite directions depending upon the cellular milieu.**

*Key words:* **CA1; dendrite; FMRP; HCN; $I_h$; PFC**

**Significance Statement**

**Changes in dendritic function, and voltage-gated ion channels in particular, are increasingly the focus of neurological disorders. We, and others, previously identified cell type-specific channelopathies in a mouse of model of Fragile X syndrome. The present study shows that replacing Fragile X Mental Retardation Protein, which is absent in Fragile X syndrome, in adult CA1 and L5 PFC neurons regulates the number of functional dendritic HCN channels in a cell type-specific manner. These results suggest that Fragile X Mental Retardation Protein regulates dendritic HCN channels via a cell-autonomous protein–protein mechanism.**

Received July 13, 2019; revised Apr. 6, 2020; accepted Apr. 15, 2020.

Author contributions: F.B., B.E.K., D.J., B.V.Z., and D.H.B. designed research; F.B., B.E.K., P.M., O.T., and D.H.B. performed research; F.B., B.E.K., P.M., B.V.Z., and D.H.B. analyzed data; F.B., B.E.K., and D.H.B. wrote the first draft of the paper; F.B., B.E.K., P.M., D.J., B.V.Z., and D.H.B. edited the paper; F.B., B.E.K., D.J., and D.H.B. wrote the paper; O.T. and B.V.Z. contributed unpublished reagents/analytic tools.

*F.B. and B.E.K. contributed equally to this work.

This work supported by National Institutes of Health Grants R01 MH100510 to D.H.B., R01 MH094839 to D.J., and Swiss National Science Foundation Grants P2ZHP3_168621 and P400PB_180785 to F.B. and a grant from the McKnight Foundation to B.V.Z. and D.J. We thank William Taylor and Eedann McCord for assistance with stereotaxic surgery.

F. Brandalise's present address: Department of Basic Neurosciences and the Center for Neuroscience, CMU, University of Geneva, 1211 Geneva, Switzerland.

B.E. Kalmbach's present address: Allen Institute for Brain Science, Seattle, WA 98109; and Department of Physiology and Biophysics, University of Washington, Seattle, WA 98195.

The authors declare no competing financial interests.

Correspondence should be addressed to Darrin H. Brager at dbrager@mail.clm.utexas.edu.

https://doi.org/10.1523/JNEUROSCI.1670-19.2020



## Introduction

Fragile X syndrome (FXS) is the most common form of inherited mental impairment and the leading identified genetic cause of autism. FXS is caused by the transcriptional silencing of the *FMR1* gene and results in the loss of a Fragile X Mental Retardation Protein (FMRP) expression. FMRP regulates protein expression through translational regulation and protein function through protein–protein interactions (Bhakar et al., 2012; M. R. Santoro et al., 2012; Brager and Johnston, 2014). There is great optimism that, because of its monogenic origin, identifying the neuropathology of FXS is attainable, which will further elucidate the etiology of mental impairment and autism more generally.

However, despite the monogenic basis of FXS, the neuronal phenotype in mice can vary across brain regions and cell types

(Brager et al., 2012; Zhang et al., 2014; Contractor et al., 2015; Kalmbach et al., 2015; Ceolin et al., 2017). The loss of FMRP results in an increase in HCN channel function in CA1 pyramidal neuron dendrites (Brager et al., 2012) but a reduction of dendritic HCN channel function in L5 pyramidal-tract (PT) projection neurons of the PFC (Zhang et al., 2014; Kalmbach et al., 2015). Nearby L5 intratelencephalic (IT) projection neurons in the PFC have no HCN channel physiological phenotype in *fmr1*$^{-/y}$ mice (Kalmbach et al., 2015). These changes in dendritic HCN channels in CA1 and PT neurons dramatically alter the integrative properties of these two neuron classes contributing to FXS mouse behavioral phenotypes (Zhang et al., 2014).

It is unclear, however, how the loss of FMRP results in differential changes in the function of the same ion channel. Changes to HCN channel function and/or expression in FXS could be caused by a primary deficiency in an FMRP-mediated intracellular process (e.g. mRNA translation or protein–protein interactions) or a secondary process extrinsic to the cell (e.g. changes in network activity and/or connectivity).

To differentiate cell-autonomous from network-level changes caused by FMRP loss, we expressed FMRP acutely in a small subset of neurons in adult *fmr1*$^{-/y}$ mice. To determine whether FMRP modulates cell properties through protein–protein contacts, we perfused neurons with purified $FMRP_{1\text{-}298}$, which displays minimal mRNA binding (Ramos et al., 2006).

Using a combination of dendritic current and voltage-clamp recordings, we show that both methods restore WT HCN channel phenotypes in hippocampal CA1 and L5 PT neurons of adult *fmr1*$^{-/y}$ mice. The fact that reintroduction of FMRP in a small number of neurons, including a single cell in the case of $FMRP_{1\text{-}298}$, restores dendritic physiology, supports the cell-autonomous regulation model of HCN channels by FMRP. We determined that FMRP was in complex with HCN channels and TRIP8b, an auxiliary protein that controls gating, surface and expression, and trafficking (B. Santoro et al., 2004). We demonstrate that, in each cell type, FMRP regulates $I_h$ density, albeit in opposite directions, by rapidly altering the number of functional channels in the dendritic membrane. We therefore conclude that FMRP regulates HCN channel function in a cell-autonomous fashion via distinct protein–protein interactions.

## Materials and Methods

*Animals.* All procedures involving animals were performed with the approval of the University of Texas Animal Care and Use Committee. All mice were housed in the satellite animal facility, under the management of the University of Texas Animal Resource Center, under reversed light/dark cycles. We used 8- to 12-week-old male WT and *Fmr1*$^{-/y}$ mice on a C57BL/6 background.

*Adeno-associated virus assembly and production.* Each recombinant adeno-associated virus construct comprised either a mouse synapsin promoter (Borghuis et al., 2011) or a rat CaMKII$\alpha$ promoter (Dittgen et al., 2004), followed by the coding sequences for mouse FMR1 gene or inducible Cre recombinase (Matsuda and Cepko, 2007) or tdTomato fluorophore, the woodchuck post-transcriptional regulatory element (WPRE), and SV40 polyadenylation sequence, and flanked by inverted terminal repeats. To impose recombinase dependence, FMR1 and tdTomato were inserted between asymmetric optimally spaced *loxP* recombination sites (Schlake and Bode, 1994). Viruses were assembled using a modified helper-free system (Stratagene) as serotype 2/1 (*rep/cap*) and purified on sequential cesium gradients according to published methods (Grieger et al., 2006). Titers were measured using a payload-independent qPCR technique (Aurnhammer et al., 2012). Typical titers were $>10^{10}$ viral genomes/µl. For coinjections, the viruses were titer-matched to equalize each in the mix. Buffer was used in place of the FMR1 vector for tdTomato-only expression.

*Stereotaxic injections.* All procedures involving animals were performed with the approval of the University of Texas Animal Care and Use Committee. Male *fmr1*$^{-/y}$ mice, 8–12 weeks old, were anesthetized with isoflurane (1%-4% mixed in oxygen), placed in a stereotaxic apparatus, and prepared for injections with craniotomies over the target injection regions. Injections were performed using a pulled glass pipette (10–15 $\mu$m diameter tip) mounted on a Nanoject II small-volume injector (Drummond Scientific). Injections were performed at a speed of 23 nl/s, separated by a 2-3 min intervals, into either the PFC (AP: 1.5 mm; ML: ±0.45 mm; DV: 2, 1.75, and 1.5 mm; 40 nl per location) or the middle hippocampus (AP: –3.4 mm; ML: ±3.5 mm; DV: 3.5, 3.25, and 3 mm; 20 nl per location). The pipette was left in place for 3–5 min before removing it from the brain. Mice were given analgesics (carprofen 5 mg/kg; TW Medical, #PF-8507) after surgery and monitored daily to ensure full recovery. Mice received a single intraperitoneal dose of 4-hydroxytamoxifen (Kühbandner et al., 2000) (45 mg/kg; Sigma Millipore, #H6278), 1 week after surgery, to induce expression of FMRP and tdTomato. Tissue was prepared for physiological and biochemical analysis 2 weeks after intraperitoneal drug administration.

*Acute slice preparation.* Mice were anesthetized with a ketamine/xylazine (100 mg/kg, 10 mg/kg) cocktail and were perfused through the heart with ice-cold saline consisting of the following (in mM): 2.5 KCl, 1.25 $NaH_2PO_4$, 25 $NaHCO_3$, 0.5 $CaCl_2$, 7 $MgCl_2$, 7 dextrose, 205 sucrose, 1.3 ascorbate, and 3 sodium pyruvate (bubbled with 95% $O_2$/5% $CO_2$ to maintain pH at ~7.4). A vibrating tissue slicer (Vibratome 3000, Vibratome) was used to make 300-$\mu$m-thick sections. For middle hippocampal slices, the brain was removed and bisected along the midline, an oblique cut was made to promote the planar orientation of the dendrites, the brain was mounted to the stage of a Vibratome, and sections were made from the middle hippocampus. For mPFC, 300 µm coronal sections were used. Slices were held for 30 minutes at 35°C in a chamber filled with aCSF consisting of the following (in mM): 125 NaCl, 2.5 KCl, 1.25 $NaH_2PO_4$, 25 $NaHCO_3$, 2 $CaCl_2$, 2 $MgCl_2$, 10 dextrose, and 3 sodium pyruvate (bubbled with 95% $O_2$/5% $CO_2$) and then at room temperature until the time of recording. WT and *fmr1*$^{-/y}$ interleaved daily when possible, although the experimenter was not blind to the genotype.

*Electrophysiology.* Slices were placed in a submerged, heated (32°C–34°C) recording chamber that was continually perfused (1-2 ml/minute) with bubbled aCSF containing the following (in mM): 125 NaCl, 3.0 KCl, 1.25 $NaH_2PO_4$, 25 $NaHCO_3$, 2 $CaCl_2$, 1 $MgCl_2$, 10 dextrose, 3 sodium pyruvate, 0.025 D-APV, 0.02 DNQX, 0.005 CGP, and 0.002 gabazine. Slices were viewed either with an Axioskop microscope (Carl Zeiss) and differential interference optics or an AxioExaminer D microscope (Carl Zeiss) and Dodt contrast optics. Patch pipettes (4–8 MΩ) were pulled from borosilicate glass and wrapped with Parafilm to reduce capacitance.

*Whole-cell recordings.* The pipette solution contained the following (in mM): 120 K-gluconate, 16 KCl, 10 HEPES, 8 NaCl, 7 $K_2$ phosphocreatine, 0.3 Na-GTP, 4 Mg-ATP, pH 7.3 with KOH. Neurobiotin (Vector Laboratories; 0.1%-0.2%) was also included for histological processing and *post hoc* cell location determination. In some experiments, $FMRP_{1\text{-}298}$ (10-100 nM; Novus Biologicals, H00002332-01) or the heat-inactivated (HI) peptide (90°C for 10 min) was included in the internal recording solution. Alexa-594 (16 $\mu$M; Thermo Fisher Scientific, #A10428) was also included in the internal recording solution to determine the dendritic recording location relative to the soma. Data were acquired using a BVC-700 amplifier (Dagan) and custom data acquisition software written using Igor Pro (Wavemetrics) or AxoGraph X (AxoGraph Scientific) data acquisition software. Data were acquired at 10–50 kHz, filtered at 2–10 kHz, and digitized by an ITC-18 (InstruTech) interface. Pipette capacitance was compensated for, and the bridge was balanced during each recording. Series resistance was monitored and compensated throughout each experiment and was 10-25 MΩ for somatic recordings and 15–40 MΩ for dendritic recordings. Recordings were discarded if series resistance increased by more than 30% during the recording. Voltages are not corrected for the liquid-junction potential (estimated as ~8 mV).

*Outside-out recordings.* Outside-out recordings were made using an Axopatch 200B amplifier (Molecular Devices), sampled at 10 kHz,

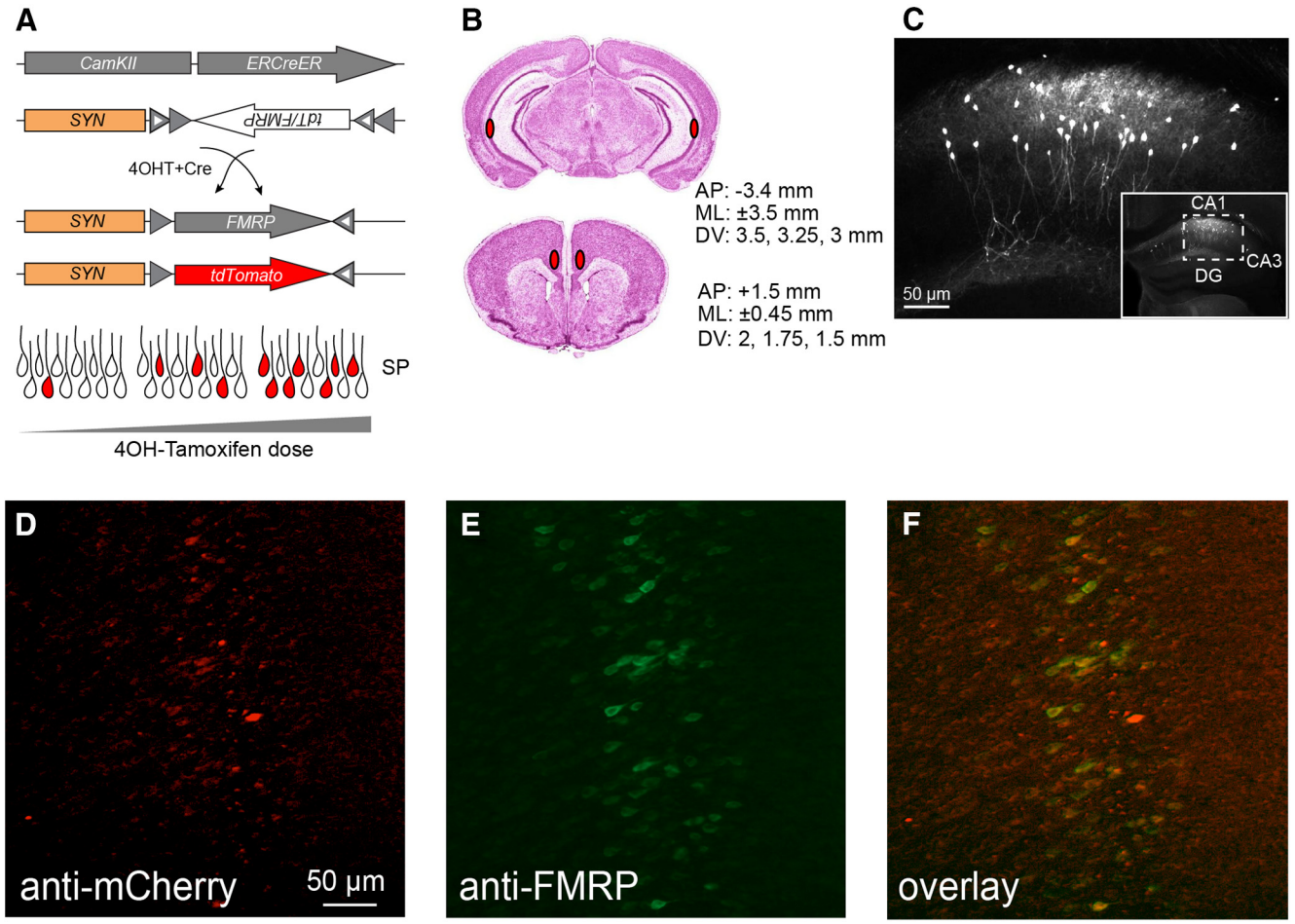


**Figure 1.** Sparse expression of FMRP. ***A***, Schematic of the sparse labeling technique: A mix of three viruses was introduced into sites shown in ***B***: one virus expressed an inactive form of Cre recombinase from a CaMKII$\alpha$ promoter, the other viruses encoded recombinase-dependent tdTomato fluorophore and FMRP (mouse FMR1 gene). Recombinase activation was dose-dependent, requiring systemic administration of 4-hydroxytamoxifen (see Materials and Methods). Protein expression was stochastic and binary. ***B***, Illustration showing the bilateral virus injection sites and stereotaxic coordinates in either the CA1 region of the hippocampus (top) or L5 of the PFC (bottom). ***C***, Representative image of a hippocampal section used for *in vitro* studies showing sparse expression of tdTomato 2 weeks following a single 4-hydroxytamoxifen injection. The CaMKII$\alpha$ promoter labeled primarily excitatory neurons but was also active in some putative stratum oriens inhibitory neurons. Recordings were performed using only excitatory neurons. Scale bar, 50 $\mu$m. ***D***, Representative fluorescent image showing the presence of tdTomato detected by anti-mCherry antibodies. ***E***, Same section as in ***D***, stained for FMRP. ***F***, Overlay of ***D*** and ***E***.

analog filtered at 2 kHz, and digitized by an ITC-18 interface connected to a computer running Axograph X. The pipette solution contained the following (in mM): 120 K-gluconate, 16 KCl, 10 HEPES, 8 NaCl, 7 $K_2$ phosphocreatine, 0.3 Na-GTP, 4 Mg-ATP, pH 7.3 with KOH. TTX (1 µM), $BaCl_2$ (0.2 mM), and $CdCl_2$ (0.1 mM) were added to the extracellular saline. $I_h$ was measured using hyperpolarizing voltage commands from –50 to –140 mV from a holding potential of –30 mV.

*Immunoprecipitation and immunohistochemistry.* The intact hippocampus was first visualized by removing subcortical tissue at the midline and then excised from the rest of the cortex. To isolate the PFC, a 1.5-mm-thick section was cut (~3-1.5 mm from bregma) and the PFC was isolated by making a diagonal cut in the cortical region above the anterior forceps of the corpus collosum toward the midline. The isolated tissues were carefully weighed. For every 100 mg of tissue, 1 ml of lysis buffer (20 mM HEPES, pH 7.4, 150 mM NaCl, 0.5% NP-40, and 0.5 mM EDTA) was added along with protease (Roche Diagnostics, #11836153001) and phosphate inhibitors (Sigma Millipore, #11836153001). The tissue was homogenized on ice using a glass Dounce homogenizer, and the lysate was clarified by centrifugation as previously described (Deng et al., 2013). Protein concentrations in the clarified lysate were typically 3–5 mg/ml. Freshly prepared lysate was used for all experiments, as protein complexes could not be reliably isolated from frozen lysate. A small fraction of the lysate was reserved as input control. Lysate was precleared with Protein G Sepharose beads (GE Healthcare, #17061802) for 1 h at 4°C. For immunoprecipitation, 10 µg of desired antibody was conjugated to 50 µl Dynabeads (Invitrogen, #00615821) in 500 µl PBS according to the manufacturer's instructions. The beads were washed with lysis buffer and rotated with the precleared lysate at 4°C for 12–16 h. The beads were washed 5 times with lysis buffer, and the associated proteins were analyzed by Western blot. Briefly, washed beads were heated in 1× Laemmli loading buffer at 80°C for 15 min, resolved on a 4%-12% NuPAGE gel, and transferred to nitrocellulose membrane (LI-COR, #926-31092). The membrane was blocked with 4% nonfat milk in PBST (10 mM PB, pH 7.4, 150 mM NaCl, 0.1% Tween 20) for 1 h and incubated at 4°C for 12 h in 1% milk in PBST with the appropriate primary antibody: anti-FMRP: 1:1000 (Cell Signaling Technology, #4317), anti-TRIP8b 1a-4 1:1000 (NeuroMab, #N212/3, RRID: AB_2750749), anti-TRIP8b 1a 1:1000 (NeuroMab, #N291C/22, RRID: AB_2315949), anti-HCN1 1:4 (NeuroMab, #73-110), anti-HCN2 1:200 (Alomone Labs, #APC-030), and anti-tubulin 1:5000 (Abcam, #EP1332Y). The membrane was washed with 2% PBST containing 2% milk and incubated for 1 h in suitable antimouse or antirabbit secondary antibody (conjugated AlexaFluor). The membrane was washed 3 times with 2% milk in PBST and 2 times with PBS before imaging on an Odyssey imaging system (LI-COR Odyssey).

To evaluate FMRP and tdTomato colocalization, mice were injected with ketamine/xylazine (10 mg/ml xylazine in 90 mg/ml ketamine) and perfused transcardially with PBS followed by 4% PFA/10 mM PB. Brains

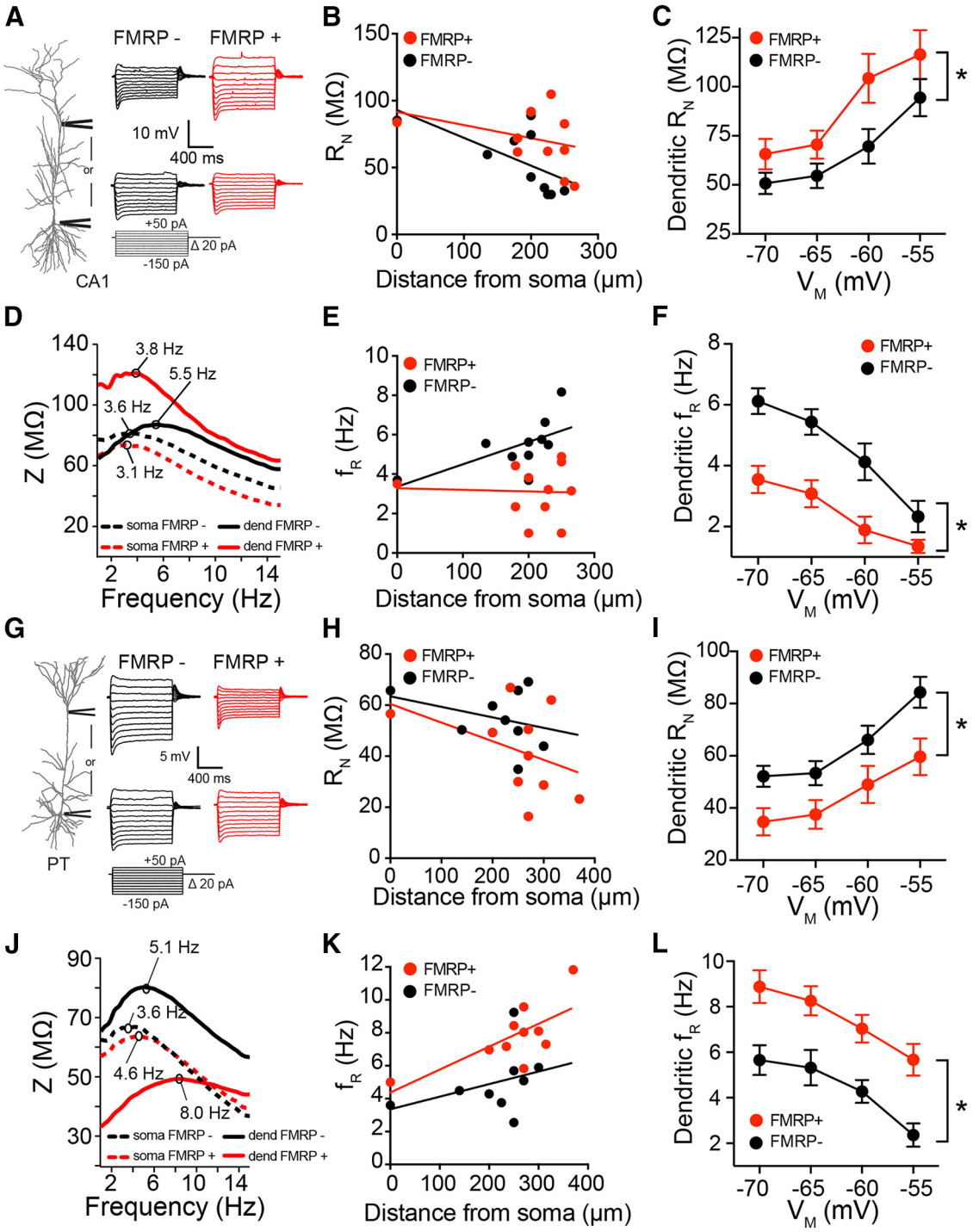


**Figure 2.** Viral replacement of FMRP restores $I_h$-related dendritic physiology in both CA1 and L5 PT *fmr1*$^{-/y}$ excitatory neurons. ***A***, Representative voltage responses to current injected into the soma or dendritic locations for both FMRP$^-$ (black) and FMRP$^+$ (red) CA1 pyramidal neurons. ***B***, Input resistance as a function of recording location for both FMRP$^-$ and FMRP$^+$ CA1 pyramidal neurons. ***C***, FMRP$^+$ CA1 neurons ($n = 9$) have a higher dendritic input resistance measured at multiple potentials compared with FMRP$^-$ neurons ($n = 9$). ***D***, Representative impedance amplitude plots in response to a chirp stimulus injected into the soma or dendritic locations for both FMRP-negative (black) and FMRP-positive (red) CA1 neurons. ***E***, Resonance frequency as a function of recording location for both FMRP$^-$ and FMRP$^+$ CA1 neurons. ***F***, FMRP$^+$ neurons have a lower dendritic resonant frequency measured at multiple potentials compared with FMRP$^-$ neurons. ***G***, Representative voltage responses to current injected into the soma or dendritic locations for both FMRP$^-$ (black) and FMRP$^+$ (red) L5 PT pyramidal neurons. ***H***, Input resistance as a function of recording location for both FMRP$^-$ and FMRP$^+$ PT pyramidal neurons. ***I***, FMRP$^+$ neurons ($n = 9$) have a lower dendritic input resistance measured at multiple potentials compared with FMRP$^-$ neurons ($n = 8$). ***J***, Representative impedance amplitude plots in response to a chirp stimulus injected into the soma or dendritic locations for both FMRP$^-$ (black) and FMRP$^+$ (red) PT neurons. ***K***, Resonance frequency as a function of recording location for both FMRP$^-$ and FMRP$^+$ PT neurons. ***L***, FMRP$^+$ neurons have a higher dendritic resonant frequency measured at multiple potentials compared with FMRP$^-$ neurons. *$p < 0.05$. Data in ***C***, ***F***, ***I***, and ***L*** presented as mean ± s.e.m.

were postfixed overnight in 4% PFA/PBS. Tissue was sectioned at 50 μm on a microtome (VT1000, Leica Microsystems) and mounted on Microfrost Plus slides (Thermo Fisher Scientific). Rehydrated sections were rinsed in PBS and incubated in sodium citrate for antigen retrieval (85°C, pH 6.0, 30 min). After the incubation, slides remained in sodium citrate until reaching room temperature. Mounted sections were rinsed in PBS and placed in blocking solution (10% normal goat serum and 0.5% Triton-X-100) at room temperature for 3 h, then rinsed and placed

in primary antibody mix (1:1 of mouse supernatant anti-FMRP, Developmental Studies Hybridoma; 1:250 goat anti-mCherry, SicGen, #AB0081; in blocking buffer) for 48 h at 4°C. The mCherry antibody to tdTomato was needed because tdTomato fluorescence diminished during antigen retrieval. Slides were washed 3 times and placed into blocking buffer with appropriate secondary antibodies (1:500 donkey anti-mouse AlexaFluor-488 #715-545-150 and 1:500 donkey anti-goat AlexaFluor-594 #715-585-151, Jackson ImmunoResearch Laboratories) for 3 h at room temperature. Slides were washed 3 times and coverslipped with Fluormount-g (Southern Biotechnology) for imaging. Images of FMRP and tdTomato immunostaining were acquired using a AxioZoomV16 microscope (Carl Zeiss) using standard Zeiss filter sets and running ZEN2pro software. Image processing and quantification were performed in Fiji (National Institutes of Health).

*Experimental design and statistical analyses.* Input resistance, sag, and rebound were calculated from the voltage response to a family of 1 s current injections (−150 to 50 pA, 20 pA steps). Input resistance was calculated from the linear portion of the current−voltage relationship. Sag was defined as the ratio of maximum to steady-state input resistance. Rebound was defined as the slope of the rebound potential as a function of steady-state membrane potential. The functional membrane time constant was defined as the slow component of a double-exponential fit of the average voltage decay in response to hyperpolarizing current injections (100-300 pA, 2 ms). Resonance was determined from the voltage response to a chirp stimulus (sinusoidal current injection that linearly increased in frequency from 1 to 15 Hz in 15 s) of constant amplitude. The impedance amplitude profile (ZAP) was constructed from the ratio of the fast Fourier transform of the voltage response to the fast Fourier transform of the current injection. The peak of the ZAP was defined as the resonant frequency. The presence (2.2 Hz) or absence of resonance was used to classify L5 mPFC neurons into projection types (PT vs IT). Patch area was estimated by fitting the decay of the capacitive transient in response to a small voltage step (assuming 1 μF $cm^{-2}$). The time constant of $I_h$ activation was estimated by fitting a single exponential to the measured current. Activation data were fit to a single Boltzmann function using a least-squares program. Linear leakage and capacitive currents were digitally subtracted by scaling traces at smaller command voltages in which no voltage-dependent current was activated.

Western blots were quantified using the Odyssey ImageLite software. Experiments where quantitation is reported were repeated at least twice using different animals and brain lysates. Differences in bound FMRP were confirmed with three experiments, four pooled brain regions per experiment. All quantified coimmunoprecipitated protein amounts were normalized against the Western blot signal of the primary immunoprecipitated protein in the pulldown. Aggregate data were then used to determine the mean and SEM. Statistical significance was determined using a paired two-tailed *t* test.

To determine protein levels in lysate, equal amounts of lysate (estimated by bicinchoninic acid assay) obtained from four pooled brain regions were resolved by SDS-PAGE and analyzed by Western blot. Protein levels were estimate using Odyssey ImageLite software and normalized against tubulin in each sample. Two independent experiments were used to obtain the mean and SEM.

*Statistical analysis.* Repeated-measures ANOVA, between-subjects factors ANOVA, mixed-factors ANOVA, and *post hoc t* tests were used to test for statistical differences between experimental conditions. Sidak's correction was used to correct for multiple comparisons. Data are presented as mean, and error bars indicate SEM. Statistical analyses were performed using Prism (GraphPad) and considered significant if $p < 0.05$. Power analyses were performed using G*power and reported as Type II error probability ($\beta$).

## Results

### Viral-mediated FMRP mosaics to examine individual neuron properties

We previously identified changes in dendritic $I_h$ using the *fmr1*$^{-/y}$ mouse model of FXS (Brager et al., 2012; Kalmbach et al., 2015). To test whether these previously published changes in HCN channel function in hippocampal pyramidal CA1 and L5 PT neurons are due to the intracellular absence of FMRP or network-wide compensatory mechanisms, we restored FMRP to small subsets of neurons in adult *fmr1*$^{-/y}$ mice using a virus-based strategy (Fig. 1*A*,*B*; see Materials and Methods).

FMRP was expressed in a mosaic, such that neighboring excitatory neurons within a small brain region were either FMRP$^+$ or FMRP$^-$. The FMRP$^+$ neurons additionally expressed a red fluorophore (tdTomato) to aid in their identification (Fig. 1*C*). To allow for expression of FMRP, electrophysiological studies were performed 2 weeks after injection. *Post hoc* immunohistochemistry confirmed the coexpression of FMRP and tdTomato (Fig. 1*D–F*). Viral expression of the fluorescent reporter tdTomato had no effect on the input resistance ($R_N$; unlabeled: 67.25 ± 4.83 MΩ; red: 64.50 ± 4.68 MΩ; *t* test labeled vs unlabeled $t = 0.4097$; df = 20; $p = 0.6864$) or resonance frequency ($f_R$; unlabeled: 3.41 ± 0.267 Hz; red: 3.74 ± 0.342 Hz; *t* test labeled vs unlabeled $t = 0.7702$; df = 20; $p = 0.4502$).

**Table 1. The effect of viral FMRP replacement on subthreshold properties of CA1 and PT neurons**

| | FMRP$^+$ ($n = 10$) | FMRP$^-$ ($n = 10$) | *p* |
|---|---|---|---|
| Viral replacement: CA1 | | | |
| $V_m$ (mV) | −63.2 ± 1.55 | −60.4 ± 1.20 | 0.17 |
| Sag | 17.9 ± 2.32 | 28 ± 2.83 | 0.0132 |
| Rebound slope (mV/mV) | −0.23 ± 0.03 | −0.4 ± 0.052 | 0.0145 |
| $\tau_M$ (ms) | 24.1 ± 3.14 | 16.6 ± 2.23 | 0.0605 |
| | FMRP$^+$ ($n = 10$) | FMRP$^-$ ($n = 8$) | *p* |
| Viral replacement: L5 PT | | | |
| $V_m$ (mV) | −59.9 ± 0.065 | −62.6 ± 0.81 | 0.0492 |
| Sag | 32.6 ± 2.98 | 21.7 ± 1.74 | 0.0135 |
| Rebound slope (mV/mV) | −0.51 ± 0.061 | −0.29 ± 0.025 | 0.0101 |
| $\tau_M$ (ms) | 8.6 ± 1.32 | 14.9 ± 1.91 | 0.0445 |

### Virally expressed FMRP restores cell-autonomous $I_h$-related dendritic properties in hippocampal excitatory CA1 and L5 PT neurons

Hippocampal CA1 pyramidal neurons in the *fmr1*$^{-/y}$ mouse have elevated dendritic $I_h$ that manifests as lower $R_N$ and higher $f_R$ compared with WT neurons (Magee, 1998; Narayanan and Johnston, 2007; Brager et al., 2012). We made whole-cell current-clamp recordings from the soma or apical dendrite of FMRP$^+$ (red, 223 ± 31 μm from soma) and FMRP$^-$ (unlabeled, 201 ± 35 μm from soma) CA1 pyramidal neurons and measured $R_N$ (Fig. 2*A-C*) and $f_R$ (Fig. 2*D-F*). Dendritic $R_N$ was significantly higher (mixed-factor ANOVA, main effect of FMRP: $F_{(1,18)} = 4.312$, $p = 0.045$, $\beta = 0.001$) and $f_R$ significantly lower (mixed-factor ANOVA, main effect of FMRP: $F_{(1,18)} = 13.62$, $p = 0.017$, $\beta = 0.001$) across multiple membrane potentials in FMRP$^+$ compared with FMRP$^-$ CA1 neurons (Fig. 2*C*,*F*). Voltage sag and rebound were also reduced and membrane time constant longer in FMRP$^+$ CA1 neurons (Table 1). The values for FMRP$^+$ and FMRP$^-$ neurons were in good agreement with WT and *fmr1*$^{-/y}$ neurons, respectively, from our previous work (Brager et al., 2012).

In contrast to CA1 neurons, the *fmr1*$^{-/y}$ dendritic phenotype in L5 PT neurons is a loss of functional $I_h$ (Kalmbach et al., 2015). We asked whether sparse expression of FMRP could rescue dendritic physiology in L5 PT neurons. We made whole-cell current-clamp recordings from the soma and dendrite of FMRP$^+$ (mean, 260 ± 71 μm from soma) and FMRP$^-$ (mean, 235 ± 48 μm from soma) L5 PT neurons. Unlike CA1, dendritic

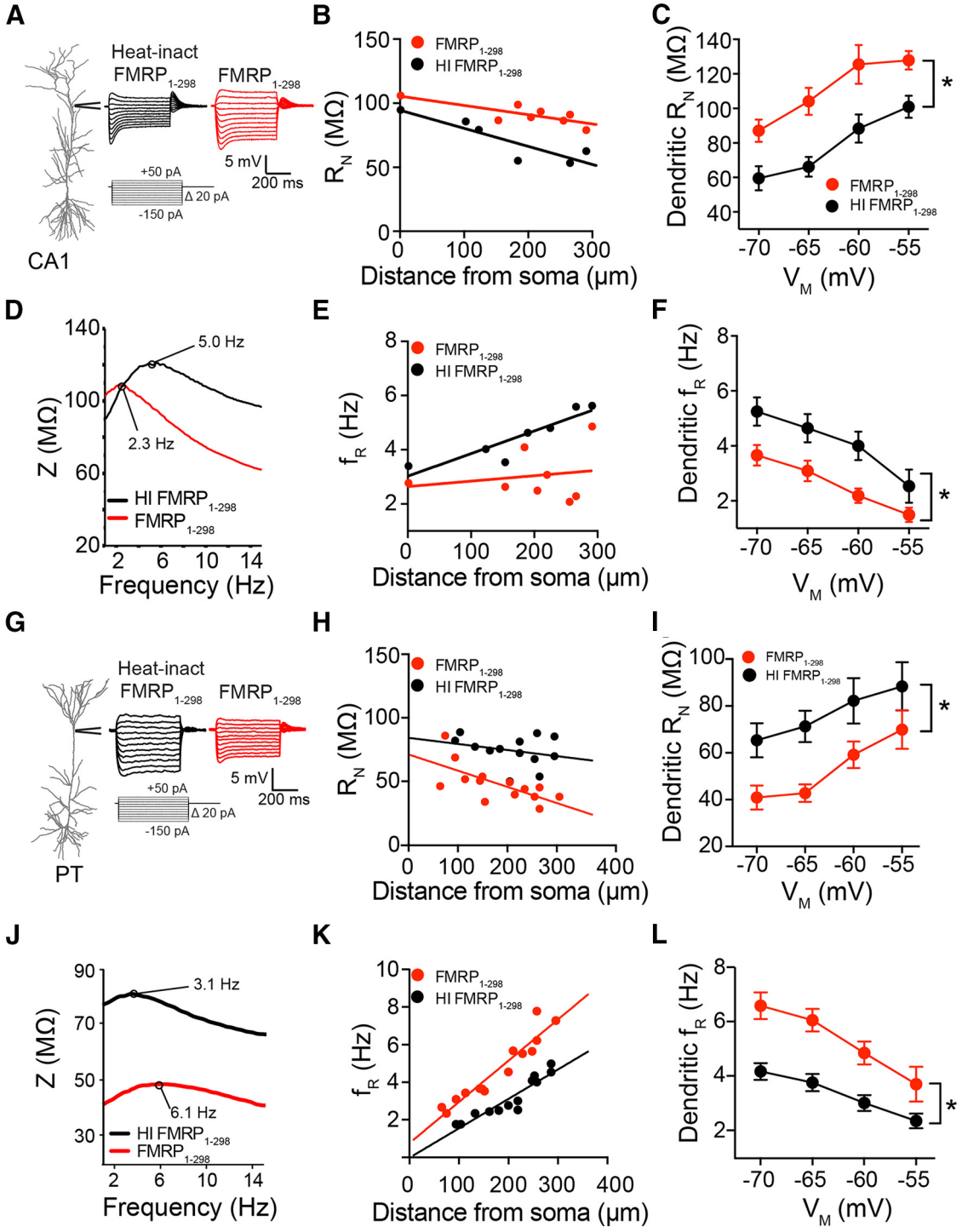


**Figure 3.** Intracellular perfusion of 100 nM $FMRP_{1–298}$ restores $I_h$-related dendritic physiology in both CA1 and L5 PT *fmr1*$^{-/y}$ excitatory neurons. ***A***, Representative voltage responses to current injected into the dendrite of *fmr1*$^{-/y}$ CA1 neurons perfused with HI $FMRP_{1–298}$ (black) and $FMRP_{1-298}$ (red). ***B***, Input resistance as a function of recording location for both HI $FMRP_{1–298}$ and $FMRP_{1–298}$. ***C***, CA1 neurons perfused with $FMRP_{1–298}$ (red, $n = 7$) have a higher dendritic input resistance measured at multiple potentials compared with HI $FMRP_{1–298}$ neurons (black, $n = 6$). ***D***, Representative impedance amplitude plots in response to a chirp stimulus injected into the CA1 dendrite using either HI $FMRP_{1–298}$ (black) or $FMRP_{1–298}$ (red). ***E***, Resonance frequency as a function of CA1 recording location for HI $FMRP_{1–298}$ (black) or $FMRP_{1–298}$ (red). ***F***, Neurons perfused with $FMRP_{1–298}$ (red) have a lower dendritic resonant frequency measured at multiple potentials compared with HI $FMRP_{1–298}$ (black). ***G***, Representative voltage responses to current injected into the L5 PT dendrite with either HI $FMRP_{1–298}$ (black) or $FMRP_{1-298}$ (red). ***H***, Input resistance as a function of recording location with either HI $FMRP_{1–298}$ (black) or $FMRP_{1-298}$ (red). ***I***, Neurons perfused with $FMRP_{1–298}$ (red, $n = 15$) have a lower dendritic input resistance measured at multiple potentials compared with neurons recorded with HI $FMRP_{1–298}$ (black, $n = 13$). ***J***, Representative impedance amplitude plots in response to a chirp stimulus injected into the dendrite using either HI $FMRP_{1–298}$ (black) or $FMRP_{1–298}$ (red). ***K***, Resonance frequency as a function of recording location for either HI $FMRP_{1–298}$ (black) or $FMRP_{1-298}$ (red). ***L***, Neurons perfused with $FMRP_{1–298}$ (red) have a higher dendritic resonant frequency measured at multiple potentials compared with HI $FMRP_{1–298}$ (black). $^*p < 0.05$. Data in ***C***, ***F***, ***I***, and ***L*** presented as mean ± s.e.m.

$R_N$ was significantly lower (mixed-factor ANOVA, main effect of FMRP: $F_{(1,13)} = 5.622$, $p = 0.0339$, $\beta = 0.001$) and $f_R$ significantly higher (mixed-factor ANOVA, main effect of FMRP: $F_{(1,13)} = 12.41$, $p = 0.0038$, $\beta = 0.001$) across multiple membrane potentials in $FMRP^+$ compared with $FMRP^-$ PT neurons (Fig. 2*G*,*L*). Voltage sag and rebound were also increased and membrane time constant shorter in $FMRP^+$ PT neurons (Table 1). The values for $FMRP^+$ and $FMRP^-$ PT neurons were in good agreement with WT and *fmr1*$^{-/y}$ neurons, respectively, from our previous work (Kalmbach et al., 2015). Together, these data demonstrate that viral expression of FMRP decreases dendritic $I_h$-related properties in *fmr1*$^{-/y}$ CA1 but increases dendritic $I_h$-related properties in *fmr1*$^{-/y}$ L5 PT neurons. Moreover, we observed only cell-autonomous, not network-level effects.

### FMRP regulates $I_h$-mediated dendritic properties in a protein–protein manner

While FMRP is traditionally considered to be a translational regulator (Darnell et al., 2005, 2011), there is evidence that FMRP can also directly interact with ion channel proteins (Brown et al., 2010; Deng et al., 2013; Zhang et al., 2014; Ferron, 2016). To test whether FMRP could affect $I_h$-related dendritic properties through protein–protein interactions and not through changes in protein expression, we perfused neurons with $FMRP_{1–298}$, a N-terminal fragment that lacks the mRNA binding domains but retains the ability to bind via protein–protein interactions (Ramos et al., 2006). The introduction of FMRP at the beginning of the recording, in contrast to 2 weeks prior, as for the previous experiments, also tested the hypothesis that the effects of FMRP replacement using viruses were likely not related to changes in protein translation. We made current-clamp recordings from *fmr1*$^{-/y}$ CA1 dendrites with 100 nM of either $FMRP_{1–298}$ or HI $FMRP_{1–298}$ included in the patch pipette. Consistent with our viral expression experiments from CA1 neurons, the inclusion of $FMRP_{1–298}$ significantly increased dendritic $R_N$ (mixed-factor ANOVA, main effect of $FMRP_{1–298}$: $F_{(1,10)} = 10.43$, $p = 0.009$, $\beta = 0.01$) and decreased $f_R$ (mixed-factor ANOVA, main effect of $FMRP_{1–298}$: $F_{(1,9)} = 8.079$, $p = 0.0193$, $\beta = 0.01$) in *fmr1*$^{-/y}$ CA1 dendrites compared with the HI control (HI $FMRP_{1–298}$; Fig. 3*A–F*). Voltage sag and rebound were also reduced and membrane time constant longer with $FMRP_{1–298}$ in the pipette (Table 2). In contrast, the inclusion of 100 nM $FMRP_{1–298}$ had the opposite effect in *fmr1*$^{-/y}$ L5 PT dendrites, decreasing $R_N$ (mixed-factor ANOVA, main effect of $FMRP_{1–298}$: $F_{(1,12)} = 6.219$, $p = 0.0282$, $\beta = 0.003$) and increasing $f_R$ (mixed-factor ANOVA, main effect of $FMRP_{1–298}$: $F_{(1,12)} = 13.86$, $p = 0.0029$, $\beta = 0.02$) (Fig. 3*G–L*). Voltage sag and rebound were also higher and membrane time constant shorter (Table 2). In all cases with $FMRP_{1–298}$ in the pipette, dendritic input resistance significantly changed within 1 min and reached steady state within 3 min of obtaining whole-cell configuration (Fig. 4) in agreement with previously published effects of $FMRP_{1–298}$ on potassium channels (Brown et al., 2010). Because the effect of perfused FMRP on cell physiology is rapid, these results indicate that $FMRP_{1–298}$, and virally expressed FMRP, can alter dendritic $I_h$ in a cell-autonomous manner, likely through protein–protein interactions.

### Replacement of FMRP does not affect PFC L5 IT neurons

In addition to PT neurons, IT neurons reside in layer 5 of the PFC and can be physiologically identified by their lack of resonance (Dembrow et al., 2010; Sheets et al., 2011; Kalmbach et al., 2015; Baker et al., 2018). We previously showed that the loss of FMRP in *fmr1*$^{-/y}$ mice selectively alters the properties of PT neurons without affecting IT neurons (Kalmbach et al., 2015). To test whether restoring FMRP expression alters the subthreshold properties of IT neurons, we made whole-cell current-clamp recordings from the soma of $FMRP^+$ and $FMRP^-$ IT neurons using the same mosaic preparation (Fig. 5*A–D*). There was no significant difference in $R_N$ (mixed-factor ANOVA, main effect of FMRP: $F_{(1,11)} = 0.4259$, $p = 0.5274$, $\beta = 0.056$) or $f_R$ (mixed-factor ANOVA, main effect of $FMRP_{1–298}$: $F_{(1,11)} = 0.4584$, $p = 0.5123$, $\beta = 0.13$) between $FMRP^+$ and $FMRP^-$ IT neurons. In agreement with these viral data, we found that recording with $FMRP_{1–298}$ or HI $FMRP_{1–298}$ had no significant effect on dendritic $R_N$ (mixed-factor ANOVA, main effect of $FMRP_{1–298}$: $F_{(1,8)} = 0.4045$, $p = 0.5426$, $\beta = 0.38$) or $f_R$ (mixed-factor ANOVA, main effect of $FMRP_{1–298}$: $F_{(1,8)} = 0.3304$, $p = 0.5812$, $\beta = 0.37$) in IT neurons (Fig. 5*E–H*). These results are in agreement with our previous conclusion that changes in the expression of FMRP have no effect on the subthreshold properties of IT neurons (Kalmbach et al., 2015).

**Table 2. The effect of $FMRP_{1-298}$ peptide on the subthreshold properties of CA1 and PT neurons**

| | $FMRP_{1-298}$ ($n = 7$) | HI $FMRP_{1-298}$ ($n = 6$) | $p$ |
|---|---|---|---|
| Peptide infusion: CA1 | | | |
| $V_m$ (mV) | −63.9 ± 0.86 | −60.4 ± 0.51 | 0.011 |
| Sag | 19 ± 3.2 | 29 ± 3.7 | 0.042 |
| Rebound slope (mV/mV) | −0.16 ± 0.034 | −0.33 ± 0.061 | 0.0263 |
| | $FMRP_{1-298}$ ($n = 14$) | HI $FMRP_{1-298}$ ($n = 11$) | $p$ |
| Peptide infusion: L5 PT | | | |
| $V_m$ (mV) | −64.5 ± 0.85 | −69.7 ± 0.83 | 0.00075 |
| Sag | 20.4 ± 1.92 | 9.1 ± 0.97 | 0.0005 |
| Rebound slope (mV/mV) | −0.193 ± 0.03 | −0.10 ± 0.015 | 0.016 |

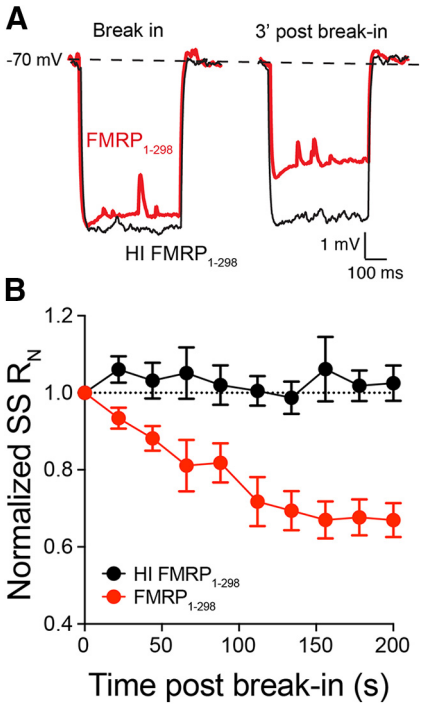


**Figure 4.** Perfusion of $FMRP_{1-298}$ rapidly alters dendritic input resistance. ***A***, Representative voltage responses to a hyperpolarizing current injection recorded with either $FMRP_{1-298}$ (red) or HI $FMRP_{1-298}$ (black) immediately after establishing a whole-cell recording and 3 min later in an L5 PT dendrite. ***B***, Summary plot showing the time course of the change in input resistance after establishing whole-cell recording with $FMRP_{1-298}$ ($n = 5$) and HI $FMRP_{1-298}$ ($n = 4$). Data presented as mean ± s.e.m.

Our initial experiments used 100 nM $FMRP_{1–298}$ based on previously published reports of FMRP regulation of $K^+$ channel function (Brown et al., 2010; Deng et al., 2013). We next asked whether lower concentrations of $FMRP_{1–298}$ could also restore normal HCN channel function. We included either 1 or 10 nM $FMRP_{1-298}$ or HI $FMRP_{1–298}$ in our pipette solution during dendritic current-clamp recordings from CA1 or L5 PT dendrites (Fig. 6). We found that 10 nM was the minimum concentration that affected dendritic physiology in both CA1 and PT dendrites (Fig. 6). We conclude that 10 nM $FMRP_{1–298}$ is sufficient to reduce dendritic $I_h$ in CA1 dendrites and increase $I_h$ in PT dendrites.

### HCN channels are in complex with FMRP and TRIP8b in WT mice

Having observed the rapid effect of perfused $FMRP_{1-298}$ on $I_h$-related dendritic physiology, we set out to determine whether FMRP is in complex with HCN channels, as was reported for FMRP and potassium channels (Brown et al., 2010; Deng et al., 2013, 2019). We used an antibody against HCN1 to immunoprecipitate HCN1 channel complexes from WT and *fmr1*$^{-/y}$ mouse hippocampus (HPC) and PFC lysates. HCN2 was present in the HPC and PFC immunoprecipitates, indicating that h channels in both the HPC and PFC from WT and *fmr1*$^{-/y}$ mice are heteromers of HCN1 and HCN2, consistent with previous reports on HCN channel composition (B. Santoro et al., 2000; Chen et al., 2001) (Fig. 7). The anti-HCN1 antibody failed to immunoprecipitate FMRP from HCN1 KO mouse extracts (not shown).

FMRP was also detected in complex with HCN1 in WT mouse lysates (Fig. 7). Despite similar levels of FMRP in the lysates from HPC and PFC (Fig. 7*C*,*D*), significantly more FMRP was found associated with HCN1 in the PFC lysate than in HPC lysate (3 ± 0.4-fold; Fig. 7*B*). The presence of FMRP associated with the HCN channel complexes supported our contention that FMRP can regulate $I_h$ through protein–protein interactions. No FMRP was detected in *fmr1*$^{-/y}$ lysates.

H channels are also known to colocalize with TPR-containing Rab8b interacting proteins (TRIP8b) (B. Santoro et al., 2004; Lewis et al., 2009; Zolles et al., 2009; Zobeiri et al., 2017). Previous studies showed the predominant TRIP8b isoforms in the hippocampus and cortex contain exon 4 (1a-4) and exon 5 (1a) (Lewis et al., 2009; B. Santoro et al., 2009).

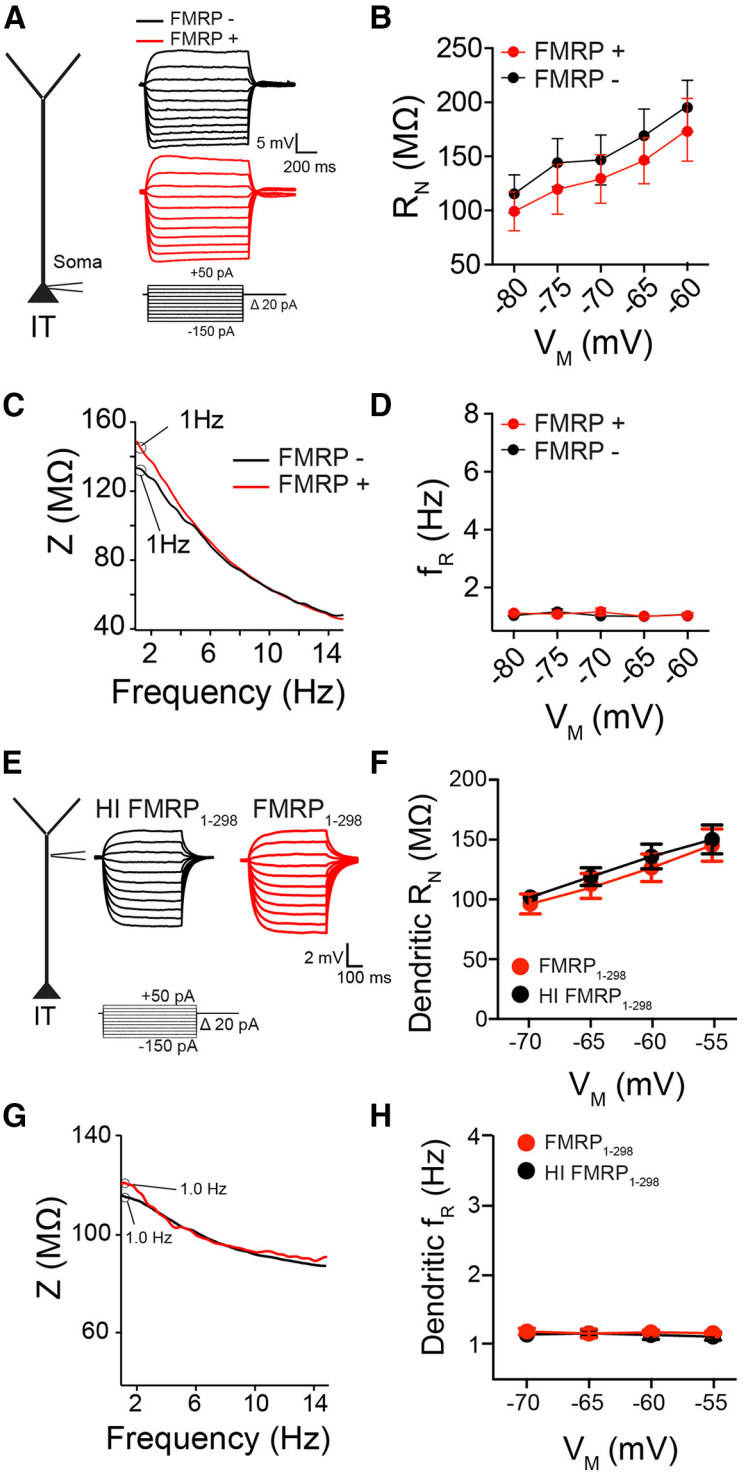


**Figure 5.** FMRP does not affect neuronal physiology of *fmr1*$^{-/y}$ L5 IT neurons. ***A***, Representative voltage responses for current injected into either a $FMRP^+$ or $FMRP^-$ IT neuron. ***B***, Summary plot showing that expression of FMRP does not affect input resistance of IT neurons ($FMRP^+$, $n = 7$; $FMRP^-$, $n = 6$). ***C***, Representative impedance amplitude profiles for a chirp stimulus injected into either a $FMRP^+$ or $FMRP^-$ IT neuron. ***D***, Summary plot showing that expression of FMRP does not affect the resonant frequency of IT neurons. ***E***, Representative voltage responses to current injected into the dendrite of *fmr1*$^{-/y}$ IT neurons perfused with HI $FMRP_{1–298}$ (black) and $FMRP_{1–298}$ (red). ***F***, $FMRP_{1–298}$ does not affect dendritic input resistance of IT neurons ($FMRP_{1–298}$, $n = 5$; HI $FMRP_{1–298}$, $n = 5$). ***G***, Representative impedance amplitude plots in response to a chirp stimulus injected into the IT dendrite using either HI $FMRP_{1–298}$ (black) or $FMRP_{1–298}$ (red). ***H***, $FMRP_{1–298}$ does not affect dendritic resonant frequency of IT neurons. Data in ***B***, ***D***, ***F*** and ***H*** presented as mean ± s.e.m.

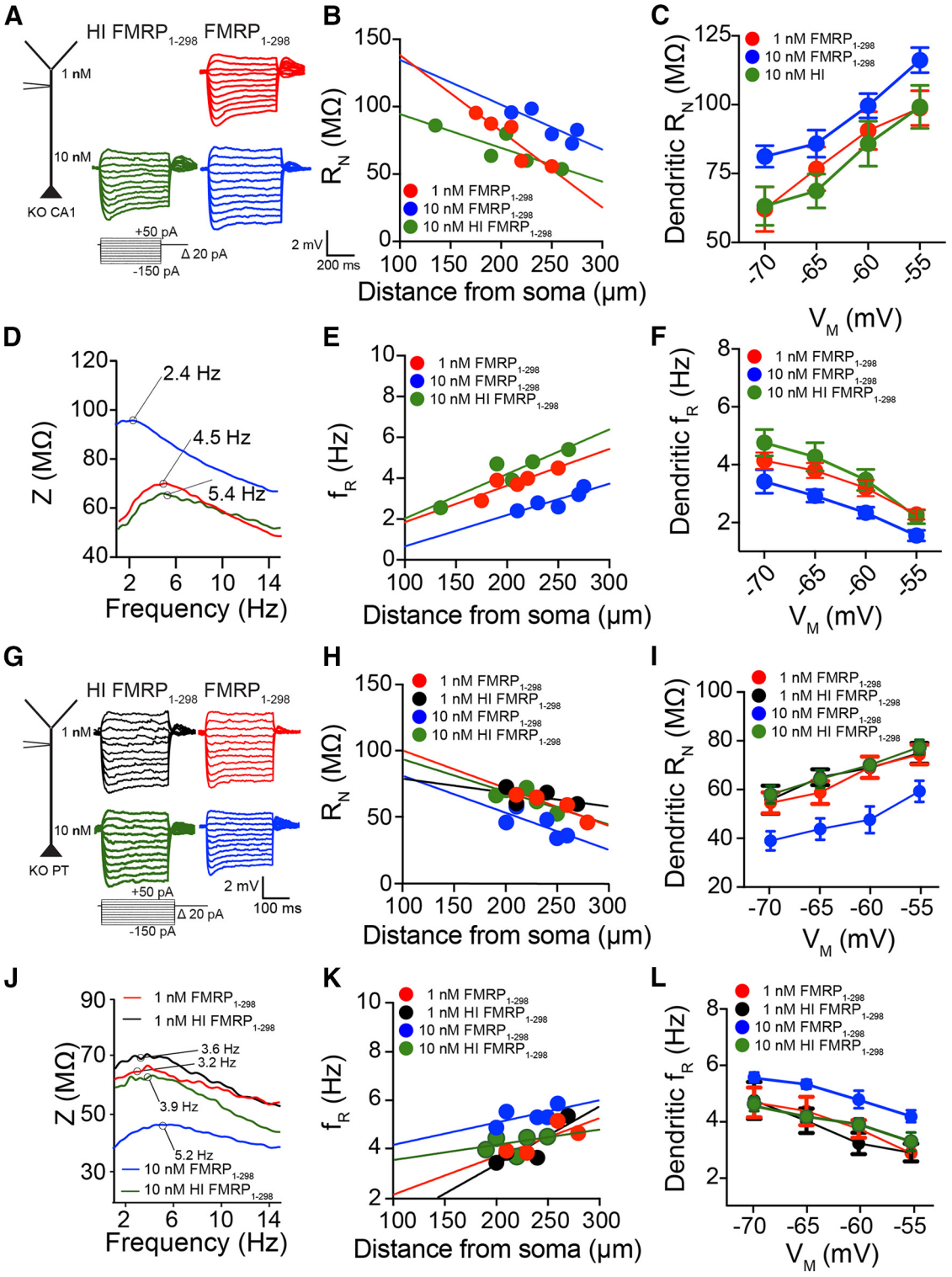


**Figure 6.** Dose-dependent effect of perfused $FMRP_{1–298}$ on dendritic function in CA1 and L5 PT *fmr1*$^{-/y}$ excitatory neurons. ***A***, Representative voltage response for current injected into the dendrite of *fmr1*$^{-/y}$ CA1 neuron recorded using 1 nM $FMRP_{1–298}$ (red, $n = 5$), 10 nM HI $FMRP_{1–298}$ (green, $n = 5$), or $FMRP_{1–298}$ (blue, $n = 5$). ***B***, Summary plot that shows input resistance as a function of recording location for 1 and 10 nM HI $FMRP_{1–298}$ and $FMRP_{1–298}$. ***C***, Only perfusion of 10 nM $FMRP_{1–298}$ (blue) reduces dendritic input resistance in *fmr1*$^{-/y}$ CA1 neurons. ***D***, Representative impedance amplitude plot for chirp stimulus injected into the dendrite of *fmr1*$^{-/y}$ CA1 neuron recorded using 1 nM HI $FMRP_{1–298}$ (black) or $FMRP_{1–298}$ (red) or 10 nM HI $FMRP_{1–298}$ (green) or $FMRP_{1–298}$ (blue). ***E***, Summary plot that shows resonant frequency as a function of recording location for 1 and 10 nM HI $FMRP_{1–298}$ and $FMRP_{1–298}$. ***F***, Only perfusion of 10 nM $FMRP_{1–298}$ (blue) increases dendritic resonant frequency in *fmr1*$^{-/y}$ CA1 neurons. ***G***, Representative voltage response for current injected into the dendrite of *fmr1*$^{-/y}$ PT neuron recorded using 1 nM HI $FMRP_{1–298}$ (black, $n = 4$) or $FMRP_{1–298}$ (red, $n = 4$) or 10 nM HI $FMRP_{1–298}$ (green, $n = 5$) or $FMRP_{1–298}$ (blue, $n = 5$). ***H***, Summary plot that shows input resistance as a function of recording location for 1 and 10 nM HI $FMRP_{1–298}$ and $FMRP_{1–298}$. ***I***, Only perfusion of 10 nM $FMRP_{1–298}$ (blue) reduces dendritic input resistance in *fmr1*$^{-/y}$ PT neurons. ***J***, Representative impedance amplitude plot for chirp stimulus injected into the dendrite of *fmr1*$^{-/y}$ PT neuron recorded using 1 nM HI $FMRP_{1–298}$ (black) or $FMRP_{1–298}$ (red) or 10 nM HI $FMRP_{1–298}$ (green) or $FMRP_{1–298}$ (blue). ***K***, Summary plot that shows resonant frequency as a function of recording location for 1 and 10 nM HI $FMRP_{1–298}$ and $FMRP_{1–298}$. ***L***, Only perfusion of 10 nM $FMRP_{1–298}$ (blue) increases dendritic resonant frequency in *fmr1*$^{-/y}$ PT neurons. Data in ***C***, ***F***, ***I*** and ***L*** presented as mean ± s.e.m.

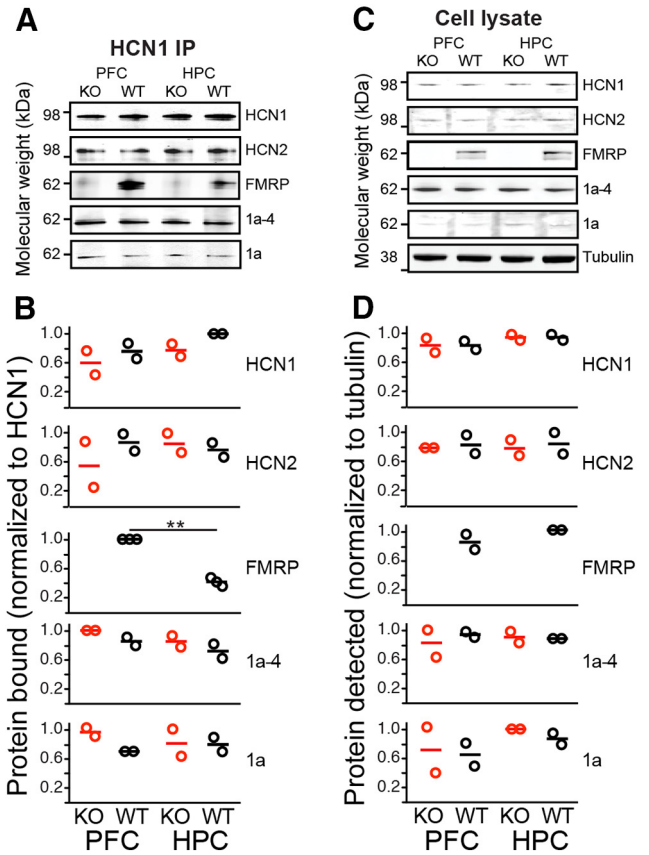


**Figure 7.** FMRP is in complex with HCN1 channel subunits. ***A***, Western blot analysis of HCN1 immunoprecipitate identified associated HCN2, FMRP, and the indicated TRIP8b isoforms. ***B***, Summary of group data shows that approximately threefold more FMRP was associated with HCN1 in the PFC compared with the HPC (three independent experiments, $p = 0.0091$). Other proteins were not significantly different across samples. Reported protein amounts were normalized to HCN1 in the precipitate. ***C***, Lysates were prepared from the indicated brain regions of WT and *fmr1*$^{-/y}$ mice, and HCN proteins, TRIP8b isoforms, FMRP, and tubulin were quantified by Western blot (see Materials and Methods). Similar lysates were used for immunoprecipitation studies. ***D***, Protein quantitation from group data normalized to tubulin. No significant differences in expression for any of the proteins could be discerned (three independent experiments for FMRP and tubulin; two experiments for HCN and TRIP8b proteins). $^{**}p < 0.01$.

In agreement, both 1a-4 and 1a were present in the HCN1 immunoprecipitates from WT and *fmr1*$^{-/y}$ mouse HPC and PFC. The quantities of both TRIP8b isoforms immunoprecipitated using an anti-HCN1 antibody and normalized based on the recovered HCN1 were similar for all sources (HPC or PFC, and WT or *fmr1*$^{-/y}$) and complex-bound proteins were enriched compared with their abundance in the lysates (Fig. 7*A*,*B*).

### FMRP regulates HCN channel conductance density

Our current-clamp data suggest that FMRP modulates $I_h$ via cell-autonomous protein–protein interactions. FMRP may regulate $I_h$ in PT and CA1 pyramidal neurons by changing HCN channel kinetics and/or density. To test for these possibilities, we pulled outside-out patches from the distal dendrites of CA1 and L5 PT neurons and made voltage-clamp recordings of $I_h$ with $FMRP_{1–298}$ in the recording pipette (Fig. 8*A*). For these experiments, outside-out patches were pulled after 3 minutes to allow for stabilization of the peptide effect on dendritic properties (Fig. 4). Consistent with previous published reports for CA1 neurons (Magee, 1998; Bittner et al., 2012), we found that $I_h$ increased with increasing distance from the soma (WT: $r^2 = 0.76$, $p = 0.0046$; $FMRP_{1–298}$: $r^2 = 0.74$, $p = 0.0059$; HI $FMRP_{1–298}$: $r^2 = 0.70$, $p = 0.0048$). However, the distance dependence and maximum $I_h$ were significantly lower with $FMRP_{1–298}$ in the pipette solution compared with HI $FMRP_{1–298}$ (mixed-factor ANOVA, interaction between membrane potential and $FMRP_{1–298}$: $F_{(18,162)} = 2.190$, $p = 0.0053$, $\beta = 0.016$; Fig. 8*A–C*). Indeed, there was no significant difference in $I_h$ between *fmr1*$^{-/y}$ dendritic patches with $FMRP_{1–298}$ and WT dendritic patches. $FMRP_{1–298}$ had no effect on the voltage dependence of $I_h$ activation (Fig. 8*D*) or activation time constant (Table 3). Similar to CA1 neurons and consistent with previous reports on L5 cortical neurons (Kole et al., 2006; Harnett et al., 2015), we found that $I_h$ increased with increasing distance from the soma in L5 PT neurons (WT: $r^2 = 0.86$, $p = 0.0076$; $FMRP_{1–298}$: $r^2 = 0.79$, $p = 0.0075$; HI $FMRP_{1–298}$: $r^2 = 0.71$, $p = 0.0167$). However, the distance dependence and maximum $I_h$ were significantly higher with $FMRP_{1–298}$ in the pipette solution compared with HI $FMRP_{1–298}$ (mixed-factor ANOVA, interaction between membrane potential and $FMRP_{1–298}$: $F_{(18,144)} = 13.37$, $p < 0.0001$, $\beta = 0.001$; Fig. 8*E–G*). Consistent with CA1 patches, $FMRP_{1–298}$ had no effect on the voltage dependence of activation (Fig. 8*H*) or activation time constant (Table 3). Thus, although FMRP regulates $I_h$ in opposite ways in CA1 versus L5 PT neurons, these voltage-clamp data, in combination with our coimmunoprecipitation results, suggest that the molecular composition of the dendritic HCN channels in CA1 and PT neurons is similar.

### FMRP regulates the number of functional dendritic h channels

Our outside-out patch-clamp experiments suggest that FMRP increases or decreases the amplitude of $I_h$ without affecting the voltage dependence or kinetics of HCN channel activation. This may occur because FMRP changes the number of available HCN channels (N) or changes the single-channel conductance ($\gamma$) of HCN channels. To distinguish between these two possibilities, we used nonstationary fluctuation analysis (NSFA) of $I_h$ measured in outside-out patches from *fmr1*$^{-/y}$ dendrites with $FMRP_{1–298}$ in the pipette (Sigworth, 1980; Kole et al., 2006). The single-channel current ($i$) and the maximum number of channels ($N$) were estimated by fitting the plot of $I_h$ current variance versus the mean $I_h$ current with a parabola (Fig. 9*A*, *B*). For both CA1 and PT dendritic patches, there was no significant difference in $\gamma$ between $FMRP_{1–298}$ and HI $FMRP_{1–298}$ (mixed-factor ANOVA, main effect of $FMRP_{1–298}$: $F_{(1,14)} = 0.7$, $\beta = 0.21$; Fig. 9*C*). In contrast, $FMRP_{1–298}$ significantly reduced $N$ in CA1 dendritic patches and significantly increased $N$ in PT dendritic patches (mixed-factor ANOVA, interaction between $FMRP_{1–298}$ and cell type: $F_{(1,14)} = 175.7$, *post hoc* Sidak's multiple comparisons test of $FMRP_{1–298}$, CA1: $p = 0.0018$, $\beta = 0.001$; PT: $p = 0.0001$, $\beta = 0.001$; Fig. 9*D*). When h channels were blocked with 20 μM ZD7288, there was a small increase in the current variance during the voltage step (baseline $\sigma^2$: 1.6 ± 0.3 pA$^2$; maximum $\sigma^2$ during step: 3.3 ± 0.5 pA$^2$; $n = 4$ patches). However, in the presence of ZD7288, the variance-current plot was not well described by a parabola and the average increase in variance was smaller compared with recordings when h channels were not blocked (105% vs 407%). These results suggest that FMRP modulates dendritic $I_h$ in both CA1 and PT neurons by rapidly decreasing and increasing the number of functional dendritic HCN channels, respectively.

## Discussion

Cortical neurons receive thousands of synaptic inputs that they can integrate and transform into action potential output. CA1

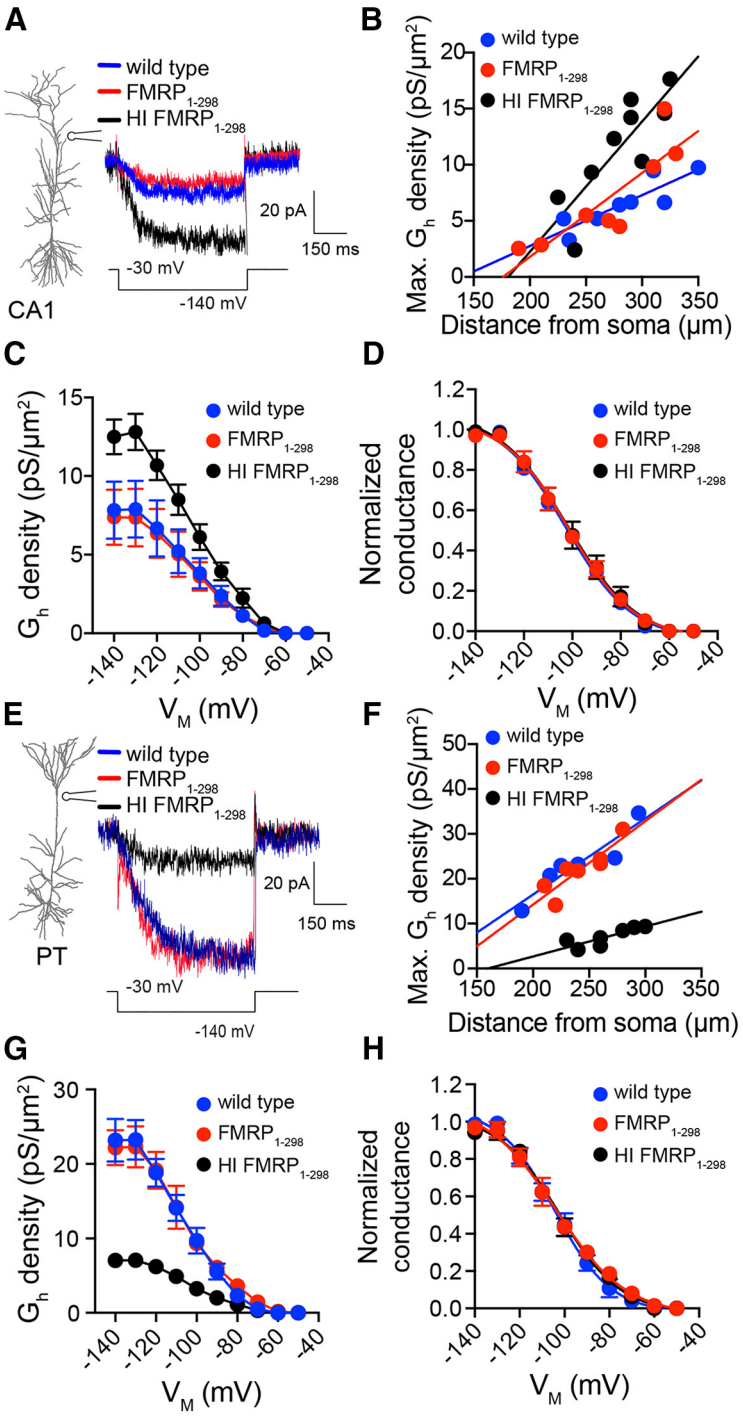


**Figure 8.** Perfused $FMRP_{1-298}$ alters current density without affecting the voltage dependence of h channels in both CA1 and L5 PT *fmr1*$^{-/y}$ excitatory neurons. ***A***, Representative recordings of the maximum $I_h$ measured in outside-out patches from WT CA1 dendrites (blue) or *fmr1*$^{-/y}$ dendrites with either HI $FMRP_{1-298}$ (black) or $FMRP_{1-298}$ (red). ***B***, Summary plot showing the maximum $I_h$ density in dendritic CA1 patches as a function of distance from the soma for WT (blue) or *fmr1*$^{-/y}$ dendrites with either HI $FMRP_{1-298}$ (black) or $FMRP_{1-298}$ (red). ***C***, Summary plot showing lower $I_h$ density as a function of membrane potential in CA1 dendritic patches from WT (blue, $n = 8$) or *fmr1*$^{-/y}$ patches measured with $FMRP_{1-298}$ (red, $n = 7$) compared with HI $FMRP_{1-298}$ (black, $n = 7$). ***D***, Summary plot showing that there was no difference in $I_h$ activation in CA1 dendritic patches from WT (blue) or *fmr1*$^{-/y}$ patches with either HI $FMRP_{1-298}$ (black) or $FMRP_{1-298}$ (red). ***E***, Representative recordings of the maximum $I_h$ measured in outside-out patches from L5 PT dendrites from WT (blue) or *fmr1*$^{-/y}$ patches with either HI $FMRP_{1-298}$ (black) or $FMRP_{1-298}$ (red). ***F***, Summary plot showing the maximum $I_h$ density in dendritic L5 PT patches as a function of distance from the soma from WT (blue, $n = 6$) or *fmr1*$^{-/y}$ patches with either HI $FMRP_{1-298}$ (black, $n = 6$) or $FMRP_{1-298}$ (red, $n = 7$). ***G***, Summary plot showing greater $I_h$ density as a function of membrane potential in L5 PT dendritic patches from WT (blue) or *fmr1*$^{-/y}$ patches measured with $FMRP_{1-298}$ (red) compared with HI $FMRP_{1-298}$ (black). ***H***, Summary plot showing that there was no difference in $I_h$ activation in L5 PT dendritic patches from WT (blue) or *fmr1*$^{-/y}$ patches with either HI $FMRP_{1-298}$ (black) or $FMRP_{1-298}$ (red). Data in ***B***, ***D***, ***G*** and ***H*** presented as mean ± s.e.m.

neurons in the hippocampus and L5 neurons in cortex have high densities of HCN channels localized in the distal dendrites (Magee, 1998; Bittner et al., 2012; Harnett et al., 2015) that can regulate the temporal and spatial integration of synaptic inputs (Harnett et al., 2013, 2015; Vaidya and Johnston, 2013; Dembrow et al., 2015). The spatial localization and unique biophysical properties of HCN channels make them critical regulators of dendritic function. Relatedly, HCN channels were implicated in several nervous system disorders, including FXS.

We previously found that dendritic $I_h$ is upregulated in CA1 dendrites but downregulated in L5 PFC dendrites in *fmr1*$^{-/y}$ mice (Brager et al., 2012; Kalmbach et al., 2015). In this study, we addressed several critical questions related to the mechanisms for these differential h channel phenotypes. Is the change in $I_h$ due to the loss of FMRP within individual neurons or a consequence of an altered neuronal network? Can the deficit be rescued after development? We found that the sparse expression of FMRP in adult CA1 and L5 PT *fmr1*$^{-/y}$ cells restored $I_h$-related properties (input resistance, resonance frequency, rebound, and sag) to WT levels. Does FMRP regulate $I_h$ via a translational or protein–protein mechanism? We also found that intracellular perfusion of a truncated FMRP lacking the C-terminal mRNA binding domains, but retaining the N-terminal protein binding domains ($FMRP_{1-298}$) is sufficient to restore dendritic h channel physiology in both cell types. This suggests that FMRP regulates HCN channel function via a protein–protein interaction. In support of this hypothesis, FMRP coimmunoprecipitates with h channel pore-forming HCN subunits and auxiliary TRIP8b subunits in both hippocampus and PFC of WT mice.

Several other ion channels are known to be in complex with FMRP and are regulated by FMRP via protein–protein interactions, including BK and SK $Ca^{2+}$-activated $K^+$ channels, $Na^+$-activated $K^+$ channels, $K_V1.2$, and N-type $Ca^{2+}$ channels (Brown et al., 2010; Deng et al., 2013, 2019; Ferron et al., 2014; Yang et al., 2018). While we did not explicitly test for interactions between $FMRP_{1-298}$ and these channels in our experiments, modulation of these channels by FMRP is unlikely to contribute to our observed changes in dendritic physiology as (1) we reported significant changes in dendritic $f_R$ in both CA1 and PT neurons, and none of these channels contributed to reso-

**Table 3. The effect of $FMRP_{1-298}$ peptide on the activation and voltage dependence of dendritic HCN channels in CA1 and PT neurons**

| | WT | KO $FMRP_{1-298}$ | KO HI $FMRP_{1-298}$ | *p* |
|---|---|---|---|---|
| CA1 dendrite | | | | |
| $\tau_{act}$ (ms) | 23.7 ± 2.17 | 23.4 ± 2.06 | 22.7 ± 1.99 | 0.872 |
| $V_{1/2}$ (mV) | −102.6 ± 1.1 | −101.7 ± 1.7 | −101.8 ± 2.1 | 0.912 |
| *k* (mV) | −13.73 ± 1.147 | −13.49 ± 1.856 | −14.4 ± 2.223 | 0.933 |
| | WT | KO $FMRP_{1-298}$ | KO HI $FMRP_{1-298}$ | *p* |
| PT dendrite | | | | |
| $\tau_{act}$ (ms) | 24.4 ± 1.22 | 23.7 ± 1.56 | 23.8 ± 1.33 | 0.929 |
| $V_{1/2}$ (mV) | −104.4 ± 1.8 | −103.7 ± 2.6 | −102.2 ± 1.7 | 0.731 |
| *k* (mV) | −12.47 ± 1.732 | −15.67 ± 2.673 | −13.67 ± 1.76 | 0.572 |

nance; (2) they are unlikely to be activated at the membrane potentials we used (–80 to –60 mV); and (3) are not expressed in significant densities in distal dendrites.

What is the cellular mechanism for the change in dendritic $I_h$? Voltage-clamp recordings from dendritic outside-out patches from both L5 PT and CA1 neurons showed that $FMRP_{1–298}$ restored dendritic HCN channel function to WT levels. We found that FMRP modulated the absolute magnitude of $I_h$, and nonstationary analysis revealed that FMRP decreased and increased the number of functional HCN channels in CA1 and PT neurons, respectively. In contrast, neither the time constant nor the voltage dependence of activation was altered by FMRP in either cell type (Table 3). Because activation kinetics are determined in part by the molecular composition of h channels, these data, together with our coimmunoprecipitation results, suggest that: (1) the molecular composition of h channels is similar between CA1 and PT neurons and (2) the absence of FMRP does not affect the makeup of dendritic h channels.

Brain region and cell type-specific deficits in neurophysiological processes occur in FXS. For example, LTD is enhanced in the CA1 region of the hippocampus but not affected in the PFC (Huber et al., 2002; Desai et al., 2006). The threshold for LTP is lower in CA1 pyramidal neurons but higher in L2/3 neurons of the PFC (Meredith et al., 2007; Routh et al., 2013). The same regional specificity is known for channelopathies. HCN channel function is higher in CA1 pyramidal neurons but reduced in L5 neurons of both the PFC and somatosensory cortex (Brager et al., 2012; Zhang et al., 2014; Kalmbach et al., 2015). A-type potassium channels are downregulated in the dendrites of CA1 pyramidal cells but upregulated at the soma of L5 PT neurons (Routh et al., 2013; Kalmbach et al., 2015). Interestingly, L5 IT neurons of the PFC had neither an $I_h$ phenotype (Kalmbach et al., 2015) nor were altered by the reintroduction of FMRP (Fig. 5). Two potential explanations for this observation are that (1) IT neurons do not express FMRP and thus have no phenotype in FMRP KO mice and/or (2) because IT neurons do not strongly express $I_h$ (Dembrow et al., 2010), the absence (or presence) of FMRP has no effect on dendritic properties sensitive to $I_h$. These two hypotheses are not mutually exclusive, and further experiments are necessary to explore this finding.

Given the multiple ways in which FMRP can regulate downstream targets (translational regulation, protein–protein interactions, mRNA transport), a single mechanism is often difficult to determine. Our data support a cell-autonomous, protein–protein-dependent mechanism by which FMRP regulates the number of functional dendritic h channels. However, a single mechanism that could account for the increase in CA1 dendrites while also reducing $I_h$ in PT dendrites is not clear. We hypothesized that FMRP could regulate the interaction between HCN

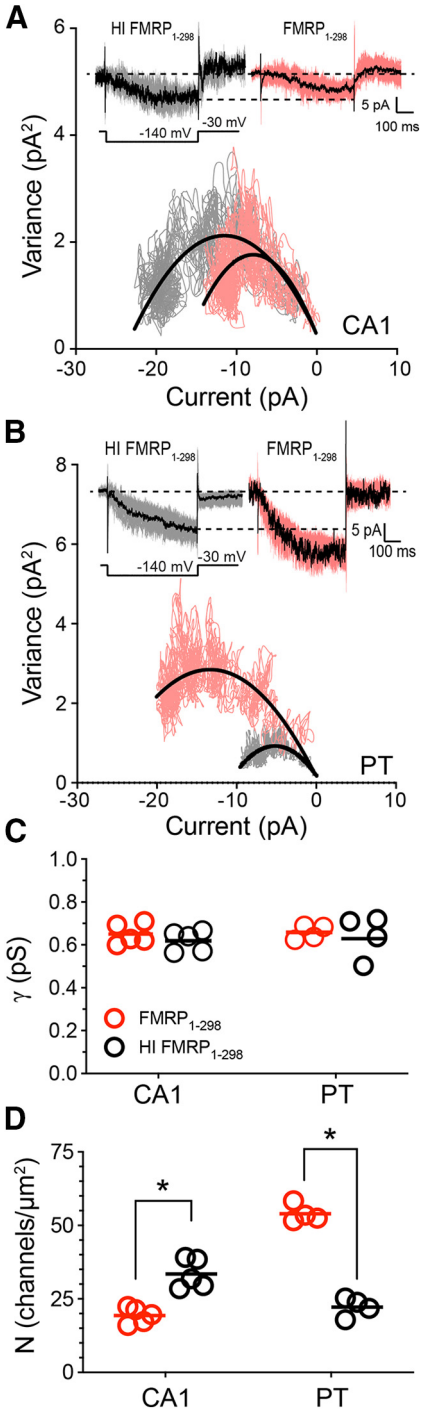


**Figure 9.** $FMRP_{1-298}$ alters the number of functional HCN channels without affecting single-channel conductance. ***A***, Variance-mean plot of h-current recordings from *fmr1*$^{-/y}$ CA1 dendritic outside-out patches showing that $FMRP_{1-298}$ (light red) decreases the number of functional HCN channels compared with HI control (gray). A parabolic function (black) was used to estimate the number of functional channels (N) and single-channel conductance ($\gamma$). Inset, Superimposed single traces used for NSFA elicited by –110 mV hyperpolarizing step (black represents the mean). ***B***, Variance-mean plot of h-current recordings from *fmr1*$^{-/y}$ PT dendritic outside-out patches showing that $FMRP_{1-298}$ (light red) increases the number of functional HCN channels compared with HI control (gray). A parabolic function (black) was used to estimate the number of functional channels (N) and single-channel conductance ($\gamma$). Inset, Superimposed single traces used for NSFA elicited by –110 mV hyperpolarizing step (black represents the mean). ***C***, Summary plot that $FMRP_{1-298}$ does not affect single-channel conductance in either CA1 or PT dendrites. ***D***, Summary plot showing that $FMRP_{1-298}$ reduces the number of functional HCN channels in CA1 patches ($n = 5, 5$) but increases the number of functional HCN channels in PT patches ($n = 4, 4$). * $p < 0.05$. Lines in ***C*** and ***D*** represent the mean.

channels and various isoforms TRIP8b. Splice variants of TRIP8b can have opposite effects on h channel surface expression and voltage dependence of activation (Lewis et al., 2009; B. Santoro et al., 2009). However, our immunoprecipitation experiments did not find a change in the association of either 1a or 1a-4 TRIP8b isoforms with HCN1 in the presence or absence of FMRP. There are three additional exon 4-containing TRIP8 splice isoforms that could be present in our immunoprecipitate that would be detected by the exon 4 antibody. They constitute <10% of total TRIP8b mRNA, however; and their action on h channel function remains unclear (B. Santoro et al., 2004). TRIP8b splice variants containing exon 1b were not detectable in our experiments (not shown). Differential regulation of adenylyl cyclase between CA1 and PT neurons, and subsequent changes in intracellular cAMP levels, could regulate the functional expression of h channels. However, cAMP-dependent modulation is typically accompanied by a shift in the voltage dependence of activation (Chen et al., 2001), which we did not observe.

Based on these results, together with the bidirectional cell type-specific regulation of HCN channel density, we hypothesize that FMRP indirectly controls $I_h$ by protein–protein-dependent regulation of an intracellular signaling pathway. Phosphorylation is one candidate for this regulatory control. In particular, activation of PKC is known to downregulate dendritic $I_h$ and reduce the number of functional h channels, whereas PKC inhibition upregulates $I_h$ (Fan et al., 2005; Brager and Johnston, 2007; Santello and Nevian, 2015; Williams et al., 2015). While FMRP is known to bind to the mRNA and regulate the translation of multiple protein kinases (Davis and Broadie, 2017), it is not clear whether FMRP is able to regulate protein phosphorylation in a protein–protein-dependent manner. To determine which components of the HCN channel complex FMRP directly binds to and how this may result in bidirectional regulation of HCN channel density requires additional experiments.

### Implications for neuronal function and treatment

Changes in dendritic HCN channel function can significantly affect how information is integrated and processed in these brain regions. CA1 and layer 5 PT pyramidal neuron dendrites are capable of generating nonlinear $Ca^{2+}$-mediated plateau potentials. In CA1 pyramidal neurons, these dendritic spikes are driven by an interaction of synaptic inputs arriving via direct input into the distal dendrites and indirect input, processed via the dentate gyrus and CA3 region, onto the more proximal dendrites. Similarly, in L5 pyramidal neurons, $Ca^{2+}$ spikes can be elicited by interactions between ascending input to basal dendrites and feedback input arriving at the apical tuft (Larkum et al., 1999a,b; Xu et al., 2012). In CA1, the higher expression of HCN channels in FXS would reduce the likelihood of nonlinear event generation and impair the induction of synaptic plasticity. Conversely, in L5 PT neurons, the lower expression of HCN channels in FXS would increase the probability of dendritic plateaus (Kole et al., 2007; Labarrera et al., 2018). Indeed, in *fmr1*$^{-/y}$ mice, L5 neurons of somatosensory cortex display increased dendritic excitability that is in part attributable to lower levels of HCN channels (Zhang et al., 2014). In addition to regulating $Ca^{2+}$ spikes, HCN channels contribute to the spectral selectivity of neurons. Specifically, HCN channels promote the integration of synaptic input containing theta frequencies. The normally high level of HCN channels expressed in the dendrites of L5 PT neurons allows them to act as temporal coincidence detectors (Dembrow et al., 2015). Only near-synchronous inputs can efficiently summate to produce local dendritic nonlinear events and drive action potential output. Thus, the spectral selectivity of CA1 and L5 PT neurons would be affected differently in FXS; CA1 neurons would be expected to prefer higher frequencies of synaptic input and L5 PT neurons lower frequencies. Intriguingly, HCN channels are more broadly expressed in pyramidal neurons across human cortical lamina compared with mouse (Kalmbach et al., 2018), potentially leading to more severe h channelopathies and FXS-related impairments in humans.

Our results shed light on how the loss of FMRP can have disparate effects on a single ion channel, depending on both the cell type and brain region. This presents a conundrum when targeting a particular deficit, including ion channels, for therapeutic intervention in Fragile X syndrome. Essentially, the targeting needs to be brain region-specific, depending on whether the behavior being addressed is hippocampal or PFC-dependent. Alternatively, broad interventions would need to target the regulation (or restoration) of the *FMR1* gene or a cellular process upstream from the effector.

## References


Aurnhammer C, Haase M, Muether N, Hausl M, Rauschhuber C, Huber I, Nitschko H, Busch U, Sing A, Ehrhardt A, Baiker A (2012) Universal real-time PCR for the detection and quantification of adeno-associated virus serotype 2-derived inverted terminal repeat sequences. Hum Gene Ther Methods 23:18–28.

Baker A, Kalmbach B, Morishima M, Kim J, Juavinett A, Li N, Dembrow N (2018) Specialized subpopulations of deep-layer pyramidal neurons in the neocortex: bridging cellular properties to functional consequences. J Neurosci 38:5441–5455.

Bhakar AL, Dölen G, Bear MF (2012) The pathophysiology of fragile X (and what it teaches us about synapses). Annu Rev Neurosci 35:417–443.

Bittner KC, Andrasfalvy BK, Magee JC (2012) Ion channel gradients in the apical tuft region of CA1 pyramidal neurons. PLoS One 7:e46652.

Borghuis BG, Tian L, Xu Y, Nikonov SS, Vardi N, Zemelman BV, Looger LL (2011) Imaging light responses of targeted neuron populations in the rodent retina. J Neurosci 31:2855–2867.

Brager DH, Akhavan AR, Johnston D (2012) Impaired dendritic expression and plasticity of h channels in the fmr1(–/y) mouse model of fragile X syndrome. Cell Rep 1:225–233.

Brager DH, Johnston D (2007) Plasticity of intrinsic excitability during long-term depression is mediated through mGluR-dependent changes in I(h) in hippocampal CA1 pyramidal neurons. J Neurosci 27:13926–13937.

Brager DH, Johnston D (2014) Channelopathies and dendritic dysfunction in Fragile X syndrome. Brain Res Bull 103:11–17.

Brown MR, Kronengold J, Gazula VR, Chen Y, Strumbos JG, Sigworth FJ, Navaratnam D, Kaczmarek LK (2010) Fragile X mental retardation protein controls gating of the sodium-activated potassium channel Slack. Nat Neurosci 13:819–821.

Ceolin L, Bouquier N, Vitre-Boubaker J, Rialle S, Severac D, Valjent E, Perroy J, Puighermanal E (2017) Cell type-specific mRNA dysregulation in hippocampal CA1 pyramidal neurons of the Fragile X syndrome mouse model. Front Mol Neurosci 10:1600.

Chen S, Wang J, Siegelbaum SA (2001) Properties of hyperpolarization-activated pacemaker current defined by coassembly of HCN1 and HCN2 subunits and basal modulation by cyclic nucleotide. J Gen Physiol 117:491–504.

Contractor A, Klyachko VA, Portera-Cailliau C (2015) Altered neuronal and circuit excitability in Fragile X syndrome. Neuron 87:699–715.

Darnell JC, Mostovetsky O, Darnell RB (2005) FMRP RNA targets: identification and validation. Genes Brain Behav 4:341–349.

Darnell JC, Van Driesche SJ, Zhang C, Hung KY, Mele A, Fraser CE, Stone EF, Chen C, Fak JJ, Chi SW, Licatalosi DD, Richter JD, Darnell RB (2011) FMRP stalls ribosomal translocation on mRNAs linked to synaptic function and autism. Cell 146:247–261.

Davis JK Broadie KB (2017) Multifarious functions of the Fragile X mental retardation protein. Trends Genet 33:703–714.

Dembrow NC, Chitwood RA, Johnston D (2010) Projection-specific neuromodulation of medial prefrontal cortex neurons. J Neurosci 30:16922–16937.

Dembrow NC, Zemelman BV, Johnston D (2015) Temporal dynamics of L5 dendrites in medial prefrontal cortex regulate integration versus coincidence detection of afferent inputs. J Neurosci 35:4501–4514.

Deng PY, Carlin D, Oh YM, Myrick LK, Warren ST, Cavalli V, Klyachko VA (2019) Voltage-independent SK channel dysfunction causes neuronal hyperexcitability in the hippocampus of Fmr1 knock-out mice. J Neurosci 39:28–43.

Deng PY, Rotman Z, Blundon JA, Cho Y, Cui J, Cavalli V, Zakharenko SS, Klyachko VA (2013) FMRP regulates neurotransmitter release and synaptic information transmission by modulating action potential duration via BK channels. Neuron 77:696–711.

Desai NS, Casimiro TM, Gruber SM, Vanderklish PW (2006) Early postnatal plasticity in neocortex of Fmr1 knockout mice. J Neurophysiol 96:1734–1745.

Dittgen T, Nimmerjahn A, Komai S, Licznerski P, Waters J, Margrie TW, Helmchen F, Denk W, Brecht M, Osten P (2004) Lentivirus-based genetic manipulations of cortical neurons and their optical and electrophysiological monitoring in vivo. Proc Natl Acad Sci USA 101:18206–18211.

Fan Y, Fricker D, Brager DH, Chen X, Lu HC, Chitwood RA, Johnston D (2005) Activity-dependent decrease of excitability in rat hippocampal neurons through increases in I(h). Nat Neurosci 8:1542–1551.

Ferron L (2016) Fragile X mental retardation protein controls ion channel expression and activity. J Physiol 594:5861–5867.

Ferron L, Nieto-Rostro M, Cassidy JS, Dolphin AC (2014) Fragile X mental retardation protein controls synaptic vesicle exocytosis by modulating N-type calcium channel density. Nat Commun 5:3628.

Grieger JC, Choi VW, Samulski RJ (2006) Production and characterization of adeno-associated viral vectors. Nat Protoc 1:1412–1428.

Harnett MT, Magee JC, Williams SR (2015) Distribution and function of HCN channels in the apical dendritic tuft of neocortical pyramidal neurons. J Neurosci 35:1024–1037.

Harnett MT, Xu NL, Magee JC, Williams SR (2013) Potassium channels control the interaction between active dendritic integration compartments in layer 5 cortical pyramidal neurons. Neuron 79:516–529.

Huber KM, Gallagher SM, Warren ST, Bear MF (2002) Altered synaptic plasticity in a mouse model of fragile X mental retardation. Proc Natl Acad Sci USA 99:7746–7750.

Kalmbach BE, Buchin A, Long B, Close J, Nandi A, Miller JA, Bakken TE, Hodge RD, Chong P, de Frates R, Dai D, Maltzer Z, Nicovich PR, Keene CD, Silbergeld DL, Gwinn RP, Cobbs C, Ko AL, Ojemann JG, Koch C, et al. (2018) h-Channels contribute to divergent intrinsic membrane properties of supragranular pyramidal neurons in human versus mouse cerebral cortex. Neuron 100:1194–1208.e1195.

Kalmbach BE, Johnston D, Brager DH (2015) Cell type-specific channelopathies in the prefrontal cortex of the $fmr1^{-/y}$ mouse model of Fragile X syndrome. eNeuro 2:ENEURO.0114-15.2015.

Kole MH, Hallermann S, Stuart GJ (2006) Single Ih channels in pyramidal neuron dendrites: properties, distribution, and impact on action potential output. J Neurosci 26:1677–1687.

Kole MH, Bräuer AU, Stuart GJ (2007) Inherited cortical HCN1 channel loss amplifies dendritic calcium electrogenesis and burst firing in a rat absence epilepsy model. J Physiol 578:507–525.

Kühbandner S, Brummer S, Metzger D, Chambon P, Hofmann F, Feil R (2000) Temporally controlled somatic mutagenesis in smooth muscle. Genesis 28:15–22.

Labarrera C, Deitcher Y, Dudai A, Weiner B, Kaduri Amichai A, Zylbermann N, London M (2018) Adrenergic modulation regulates the dendritic excitability of layer 5 pyramidal neurons in vivo. Cell Rep 23:1034–1044.

Larkum ME, Kaiser KM, Sakmann B (1999a) Calcium electrogenesis in distal apical dendrites of layer 5 pyramidal cells at a critical frequency of back-propagating action potentials. Proc Natl Acad Sci USA 96:14600–14604.

Larkum ME, Zhu JJ, Sakmann B (1999b) A new cellular mechanism for coupling inputs arriving at different cortical layers. Nature 398:338–341.

Lewis AS, Schwartz E, Chan CS, Noam Y, Shin M, Wadman WJ, Surmeier DJ, Baram TZ, MacDonald RL, Chetkovich DM (2009) Alternatively spliced isoforms of TRIP8b differentially control h channel trafficking and function. J Neurosci 29:6250–6265.

Magee JC (1998) Dendritic hyperpolarization-activated currents modify the integrative properties of hippocampal CA1 pyramidal neurons. J Neurosci 18:7613–7624.

Matsuda T, Cepko CL (2007) Controlled expression of transgenes introduced by in vivo electroporation. Proc Natl Acad Sci USA 104:1027–1032.

Meredith RM, Holmgren CD, Weidum M, Burnashev N, Mansvelder HD (2007) Increased threshold for spike-timing-dependent plasticity is caused by unreliable calcium signaling in mice lacking fragile X gene FMR1. Neuron 54:627–638.

Narayanan R, Johnston D (2007) Long-term potentiation in rat hippocampal neurons is accompanied by spatially widespread changes in intrinsic oscillatory dynamics and excitability. Neuron 56:1061–1075.

Ramos A, Hollingworth D, Adinolfi S, Castets M, Kelly G, Frenkiel TA, Bardoni B, Pastore A (2006) The structure of the N-terminal domain of the fragile X mental retardation protein: a platform for protein–protein interaction. Structure 14:21–31.

Routh BN, Johnston D, Brager DH (2013) Loss of functional A-type potassium channels in the dendrites of CA1 pyramidal neurons from a mouse model of Fragile X syndrome. J Neurosci 33:19442–19450.

Santello M, Nevian T (2015) Dysfunction of cortical dendritic integration in neuropathic pain reversed by serotoninergic neuromodulation. Neuron 86:233–246.

Santoro B, Chen S, Lüthi A, Pavlidis P, Shumyatsky GP, Tibbs GR, Siegelbaum SA (2000) Molecular and functional heterogeneity of hyperpolarization-activated pacemaker channels in the mouse CNS. J Neurosci 20:5264–5275.

Santoro B, Wainger BJ, Siegelbaum SA (2004) Regulation of HCN channel surface expression by a novel C-terminal protein–protein interaction. J Neurosci 24:10750–10762.

Santoro B, Piskorowski RA, Pian P, Hu L, Liu H, Siegelbaum SA (2009) TRIP8b splice variants form a family of auxiliary subunits that regulate gating and trafficking of HCN channels in the brain. Neuron 62:802–813.

Santoro MR, Bray SM, Warren ST (2012) Molecular mechanisms of fragile X syndrome: a twenty-year perspective. Annu Rev Pathol 7:219–245.

Schlake T, Bode J (1994) Use of mutated FLP recognition target (FRT) sites for the exchange of expression cassettes at defined chromosomal loci. Biochemistry 33:12746–12751.

Sheets PL, Suter BA, Kiritani T, Chan CS, Surmeier DJ, Shepherd GM (2011) Corticospinal-specific HCN expression in mouse motor cortex: Ih-dependent synaptic integration as a candidate microcircuit mechanism involved in motor control. J Neurophysiol 106:2216–2231.

Sigworth FJ (1980) The variance of sodium current fluctuations at the node of Ranvier. J Physiol 307:97–129.

Vaidya SP, Johnston D (2013) Temporal synchrony and gamma-to-theta power conversion in the dendrites of CA1 pyramidal neurons. Nat Neurosci 16:1812–1820.

Williams AD, Jung S, Poolos NP (2015) Protein kinase C bidirectionally modulates Ih and hyperpolarization-activated cyclic nucleotide-gated (HCN) channel surface expression in hippocampal pyramidal neurons. J Physiol 593:2779–2792.

Xu NL, Harnett MT, Williams SR, Huber D, O'Connor DH, Svoboda K, Magee JC (2012) Nonlinear dendritic integration of sensory and motor input during an active sensing task. Nature 492:247–251.

Yang YM, Arsenault J, Bah A, Krzeminski M, Fekete A, Chao OY, Pacey LK, Wang A, Forman-Kay J, Hampson DR, Wang LY (2018) Identification of a molecular locus for normalizing dysregulated GABA release from interneurons in the Fragile X brain. Mol Psychiatry. Advance online publication. Retrieved September 17, 2018. doi: 10.1038/s41380-018-0240-0.

Zhang Y, Bonnan A, Bony G, Ferezou I, Pietropaolo S, Ginger M, Sans N, Rossier J, Oostra B, LeMasson G, Frick A (2014) Dendritic channelopathies contribute to neocortical and sensory hyperexcitability in Fmr1(–/y) mice. Nat Neurosci 17:1701–1709.

Zobeiri M, Chaudhary R, Datunashvili M, Heuermann RJ, Lüttjohann A, Narayanan V, Balfanz S, Meuth P, Chetkovich DM, Pape HC, Baumann A, van Luijtelaar G, Budde T (2017) Modulation of thalamocortical oscillations by TRIP8b, an auxiliary subunit for HCN channels. Brain Struct Funct 556:1–28.

Zolles G, Wenzel D, Bildl W, Schulte U, Hofmann A, Müller CS, Thumfart JO, Vlachos A, Deller T, Pfeifer A, Fleischmann BK, Roeper J, Fakler B, Klöcker N (2009) Association with the auxiliary subunit PEX5R/Trip8b controls responsiveness of HCN channels to cAMP and adrenergic stimulation. Neuron 62:814–825.